Cancer Science
The official journal of the Japanese Cancer Association

# Leukemic T cells are specifically enriched in a unique $CD3^{dim}CD7^{low}$ subpopulation of $CD4^+$ T cells in acute-type adult T-cell leukemia

Yamin Tian,[1,2] Seiichro Kobayashi,[1] Nobuhiro Ohno,[3] Masamichi Isobe,[3] Mayuko Tsuda,[3] Yuji Zaike,[4] Nobukazu Watanabe,[5] Kenzaburo Tani,[2] Arinobu Tojo[1,3] and Kaoru Uchimaru[3,6]

[1]Division of Molecular Therapy, Institute of Medical Science, The University of Tokyo, Tokyo; [2]Department of Molecular Genetics, Medical Institute of Bioregulation, Kyushu University, Fukuoka; [3]Department of Hematology/Oncology; [4]Clinical Laboratory, Research Hospital; [5]Laboratory of Diagnostic Medicine, Division of Stem Cell Therapy, Institute of Medical Science, The University of Tokyo, Tokyo, Japan

(Received July 27, 2010/Revised November 1, 2010/Accepted December 8, 2010/Accepted manuscript online December 14, 2010/Article first published online January 23, 2011)

**The morphological discrimination of leukemic from non-leukemic T cells is often difficult in adult T-cell leukemia (ATL) as ATL cells show morphological diversity, with the exception of typical "flower cells." Because defects in the expression of CD3 as well as CD7 are common in ATL cells, we applied multi-color flow cytometry to detect a putative leukemia-specific cell population in the peripheral blood from ATL patients. $CD4^+CD14^-$ cells subjected to two-color analysis based on a CD3 *vs* CD7 plot clearly demonstrated the presence of a $CD3^{dim}CD7^{low}$ subpopulation in each of nine patients with acute-type ATL. The majority of sorted cells from this fraction showed a flower cell-like morphology and carried a high proviral load for the human T-cell leukemia virus type 1 (HTLV-I). Genomic integration site analysis (inverse long-range PCR) and analysis of the T cell receptor Vβ repertoire by flow cytometry indicated that the majority of leukemia cells were included in the $CD3^{dim}CD7^{low}$ subpopulation. These results suggest that leukemic T cells are specifically enriched in a unique $CD3^{dim}CD7^{low}$ subpopulation of $CD4^+$ T cells in acute-type ATL. (*Cancer Sci* 2011; 102: 569–577)**

Adult T-cell leukemia (ATL) is a malignant disorder caused by human T-cell leukemia virus type 1 (HTLV-I)[1] and is characterized clinically by generalized lymphadenopathy, hepatosplenomegaly, skin lesions, hypercalcemia and a characteristic morphology termed "flower cells." Importantly, ATL is one of the most incurable lymphoid malignancies. This disease is endemic to several regions in the world, including sub-Saharan Africa, the Caribbean basin, South America and Japan, and 10–20 million people are estimated to be infected by this virus worldwide.[2,3]

Evaluation of the response after chemotherapy for ATL partly depends on the proportion of ATL cells in the peripheral blood. However, the morphological diversity of ATL cells may lead to inaccurate estimations. Accurate estimation of the chemotherapeutic effect is pivotal in clinical practice because ATL cells often become chemoresistant, even during chemotherapy. Methods to detect ATL cells with greater precision than morphological examination are therefore required.

Aberrant expression of cell-surface antigens in myeloid/lymphoid leukemia cells has been studied extensively.[4–6] Using fluorescence-activated cell sorting (FACS) analysis, gating cells with diminished CD45 expression in acute myeloid/lymphoid leukemia is widely used for purifying leukemia cells. However, in ATL there are only limited data regarding the identification of transformed leukemia cells by similar methods. Previous studies indicated that most ATL cells lack CD7 and exhibit diminished CD3 expression.[7–10] Although a study using CD3 gating by FACS analysis has indicated that ATL cells were distinguishable from normal lymphocytes as a $CD3^{low}$ population,[f0] these cells were not well characterized as ATL cells.

In the present study, we focused on the enrichment of ATL cells by constructing CD3 *vs* CD7 plots from multi-color FACS. $CD3^{dim}CD7^{dim}$ and $CD3^{dim}CD7^{low}$ cells were extensively studied and compared with normal control samples. Taken together, our data suggest that ATL cells are purified in $CD3^{dim}CD7^{low}$ subpopulations. The purification of ATL cells by FACS may therefore allow monitoring of disease activity and yield insight into the biology of this disease.

## Materials and Methods

**Cell lines and patient samples.** TL-Om1, a HTLV-I-infected cell line, was provided by Dr. Toshiki Watanabe (The University of Tokyo), and was cultured in RPMI 1640 medium containing 10% fetal bovine serum. Peripheral blood samples were collected from patients admitted to our hospital (Research Hospital, Institute of Medical Science, The University of Tokyo, Tokyo, Japan) during the period from August 2009 to April 2010 with written informed consent. All patients were diagnosed with acute-type ATL according to Shimoyama's criteria.[8] Blood samples were collected before treatment using the LSG15 protocol[11] or during the recovery phase between chemotherapy sessions. Samples collected from five healthy volunteers (median age, 45 years) were used as normal controls. The present study was approved by the institutional review board of our hospital.

**Flow cytometry and cell sorting.** Peripheral blood mononuclear cells (PBMC) were isolated from heparin-treated whole blood by density gradient centrifugation using Lymphoprep (Axis-Shield, Dundee, UK) and subsequently suspended in phosphate-buffered saline (PBS) containing 5% mouse serum (DAKO, Glostrup, Denmark) for prevention of nonspecific antibody binding. Cells were stained using a combination of phycoerythrin (PE)-CD7, PE-Cy7-CCR4, allophycocyanin (APC)-CD25, APC-Cy7-CD3, Pacific Blue-CD4 and Pacific Orange-CD14. Pacific Orange-CD14 was purchased from Caltag-Invitrogen (Carlsbad, CA, USA). All other antibodies were obtained from BD BioSciences (San Jose, CA, USA). Propidium iodide (PI; Sigma, St Louis, MO, USA) was added to the samples to stain dead cells immediately prior to FACS analysis. Cells were also stained with APC-FoxP3 (eBioscience, San Diego, CA, USA) using intracellular staining methods as previously described.[12] A TCR-Vβ repertoire kit (Beckman Coulter, Miami, FL, USA) was used for T-cell receptor (TCR) Vβ repertoire analysis according to the manufacturer's instructions.

[6]To whom correspondence should be addressed.
E-mail: uchimaru@ims.u-tokyo.ac.jp

doi: 10.1111/j.1349-7006.2010.01833.x

A BD FACS Aria (BD Immunocytometry Systems, San Jose, CA, USA) was used for all multi-color FACS analysis and cell sorting. Data were analyzed using FlowJo software (Treestar, San Carlos, CA, USA).

**Quantification of HTLV-I proviral load by real-time quantitative polymerase chain reaction (PCR).** The HTLV-I proviral load in PBMC was quantified by real-time quantitative polymerase chain reaction (PCR; TaqMan method) using the ABI Prism 7000 sequence detection system (Applied Biosystems, Foster City, CA, USA) as previously described.[13] Briefly, a total of 50 ng of genomic DNA was extracted from human PBMC using a QIAamp DNA blood Micro kit (Qiagen, Hilden, Germany). Triplicate samples of the DNA were amplified. Each PCR mixture containing a HTLV-I pX region-specific primer pair at 0.1 μM (forward primer 5′-CGGATACCCAGTCTACGTGTT-3′ and reverse primer 5′-CAGTAGGGCGTGACGATGTA-3′), FAM-labeled probe at 0.1 μM (5′- CTGTGTACAAGGC-GACTGGTGCC-3′) and 1× TaqMan Universal PCR master mix

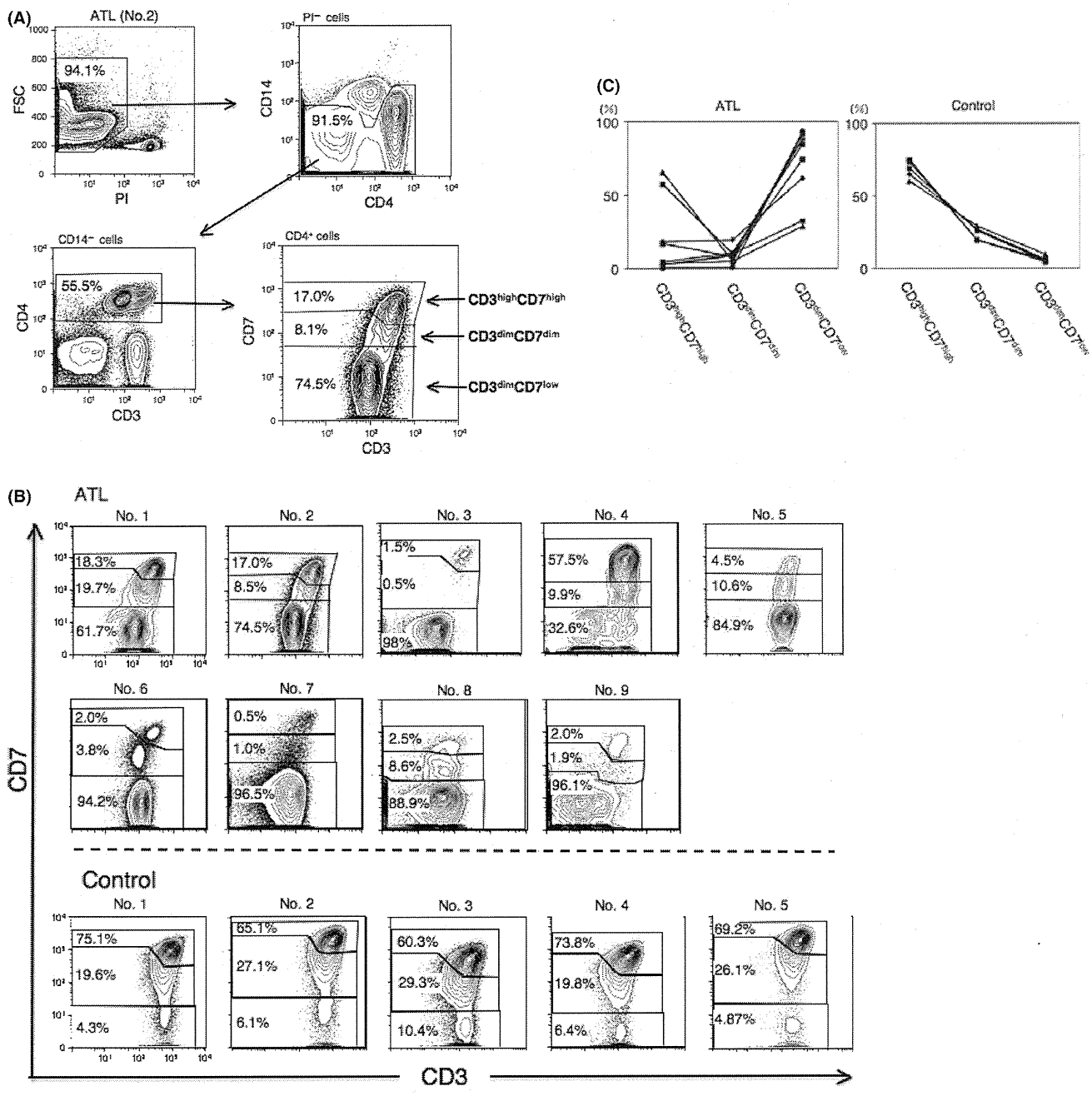


**Fig. 1.** CD3 *vs* CD7 plots from FACS analysis of patients with acute-type adult T-cell leukemia (ATL) and normal controls. (A) Representative flow cytometric analysis of a patient with acute-type ATL (patient no. 2). The CD3 *vs* CD7 plot in $CD4^+$ cells was constructed according to the gating procedure shown in this figure. In the plot, we designated three subpopulations: $CD3^{high}CD7^{high}$, $CD3^{dim}CD7^{dim}$ and $CD3^{dim}CD7^{low}$. (B) Flow cytometric profile of the CD3 *vs* CD7 plot in patients with acute-type ATL and normal controls. (C) Percentages of $CD3^{high}CD7^{high}$, $CD3^{dim}CD7^{dim}$ and $CD3^{dim}CD7^{low}$ subpopulations in $CD4^+$ T cells in patients with acute-type ATL and normal controls. Each line represents an individual sample. ATL group, $n = 9$; control group, $n = 5$; FSC, forward scatter; PI, Propidium iodide.



doi: 10.1111/j.1349-7006.2010.01833.x

**Table 1. Clinical profile of nine acute-type ATL patients in the present study**

| No. | Age | Sex | WBC (/μL) | Lymph (%) | ATL cells† (%) | Organ involvement |
|---|---|---|---|---|---|---|
| 1 | 60 | M | 5200 | 15.0 | 11.0 | Skin |
| 2 | 69 | F | 1600 | 43.5 | 9.0 | Liver, LN, pleural effusion |
| 3 | 61 | M | 18 620 | 24.7 | 43.7 | Liver, uvea |
| 4 | 59 | F | 6420 | 8.5 | 0.0 | Liver, LN, skin |
| 5 | 70 | F | 290 | 56.0 | 2.0 | Liver, spleen, LN |
| 6 | 60 | F | 4570 | 19.0 | 73.0 | Skin |
| 7 | 53 | F | 12 210 | 11.0 | 52.0 | LN |
| 8 | 74 | F | 6480 | 16.5 | 25.5 | Liver, spleen, LN |
| 9 | 63 | F | 34 810 | 21.5 | 33.5 | Liver, spleen, LN, lung |

†Proportion of ATL cells in the peripheral blood WBC evaluated by morphological examination. ATL, adult T-cell leukemia; LN, lymph nodes; Lymph, lymphocytes; WBC, white blood cells (normal range, 3500–9100/μL).

(Applied Biosystems) were subjected to 50 cycles of denaturation (95°C, 15 s) and annealing to extension (60°C, 1 min), following an initial Taq polymerase activation step (95°C, 10 min). The RNase P control reagent (Applied Biosystems) was used as an internal control for calculation of the input cell number (using VIC reporter dye). DNA extracted from TL-Om1 and normal human PBMC were used as positive and negative controls, respectively. The HTLV-I proviral load (%) was calculated as the copy number of the pX region per input cell number. To correct the deviation of acquired data in each experiment, data from TL-Om1 (positive control) were adjusted to 100% and the sample data was corrected by proportional calculation accordingly.

**Inverse long PCR.** For clonality analysis, inverse long PCR was performed. First, 1 μg of genomic DNA extracted from the FACS-sorted cells was digested with *Eco*RI, *Hin*dIII and *Pst*I at 37°C overnight. Purification of DNA fragments was performed using a QIAEX2 gel extraction kit (Qiagen). The purified DNA was self-ligated with T4 DNA ligase (Takara Bio, Otsu, Japan) at 16°C overnight. The circular DNA obtained from the *Eco*RI digestion fragment was then digested with *Mlu*I, which cuts the pX region of the HTLV-I genome and prevents amplification with the viral genome. Inverse long PCR was performed using Takara LA *Taq* polymerase (Takara Bio). The primer pairs for the *Eco*RI-treated template were: forward primer 5′-TGCCTGACCCTGCTTGCTCAACTCTACGTCTTTG-3′ and reverse primer 5′-AGTCTGGGCCCTGACCTTTTCAGACTTCTGTTTC-3′. For the *Hin*dIII-treated group, forward primer 5′-TAGCAGGAGTCTATAAAAGCGTGGAGACAG-3′ and reverse primer 5′-TGGGCAGGATTGCAGGGTTTAGAGTGG-3′ were used. For the *Pst*I-treated group, forward primer 5′-CAGCCCATTCTATAGCACTCTCCAGGAGAG-3′ and reverse primer 5′-CAGTCTCCAAACACGTAGACTGGGTATCCG-3 were used. Each 50-μL reaction mixture contained 0.4 mM of each dNTP, 25 mM $MgCl_2$, 10× LA PCR buffer II containing 20 mM Tris–HCl and 100 mM KCl, 0.5 mM primer, 2.5 U LA *Taq* polymerase and 50 ng of the processed genomic DNA. The reaction mixture of the *Eco*RI- or *Pst*I-treated group was subjected to 35 cycles of denaturation (94°C, 30 s) and annealing to extension (68°C, 8 min). For the *Hin*dIII group, the PCR conditions were denaturation (98°C, 30 s), annealing to extension (64°C, 10 min) for 5 cycles, followed by 30 cycles of denaturation (94°C, 30 s), annealing (64°C, 3 min) and extension (72°C, 15 min). Following PCR, the products were subjected to electrophoresis in 0.8% agarose gels. In the $CD3^{dim}CD7^{low}$ subpopulation from which a sufficient amount of DNA was extracted, PCR were performed in duplicate.

**Cytospin and May–Giemsa staining.** Cells enriched by cell sorting were washed twice with PBS. Aliquots of 100 μL of the cell suspension were mixed with 20 μL of 10% bovine serum albumin. The mixtures were centrifuged at 20*g* for 5 min onto glass slides. The fixed cells were air-dried and then subjected to May–Giemsa staining.

**Statistical analyses.** Data are expressed as the means ± standard deviation (SD). One-way analysis of variance (ANOVA) was used for statistical analyses, and $P < 0.05$ was taken to indicate statistical significance.

## Results

**Multi-color FACS, including CD3 *vs* CD7 plots, in patients with acute-type ATL.** We constructed a gating procedure for flow cytometric analysis of acute-type ATL cells using a combination of CD3 and CD7. Figure 1A shows the representative flow cytometric data of an ATL sample (from patient no. 2 in Table 1). Dead cells (PI positive) were initially excluded on the forward scatter (FSC) *vs* PI plot. Next, monocytes ($CD4^{dim}$ $CD14^{+}$) were excluded on the CD4 *vs* CD14 plot. After $CD4^{+}$ T lymphocytes were gated on the CD3 *vs* CD4 plot, a CD3 *vs* CD7 plot was constructed. Based on the cell density and fluorescence intensity of CD3 and CD7, we designated three subpopulations on this plot: $CD3^{high}CD7^{high}$, $CD3^{dim}CD7^{dim}$ and $CD3^{dim}CD7^{low}$ (Fig. 1A). Using the same gating procedure, we analyzed nine patients with acute-type ATL and five normal controls (Fig. 1B). The patient characteristics analyzed in the present study are shown in Table 1. In normal controls, the expression pattern of CD3 *vs* CD7 was similar. The highest cell density was observed in the $CD3^{high}CD7^{high}$ subpopulation, and the $CD3^{dim}CD7^{dim}$ subpopulation was observed adjacent to it. The $CD3^{dim}CD7^{low}$

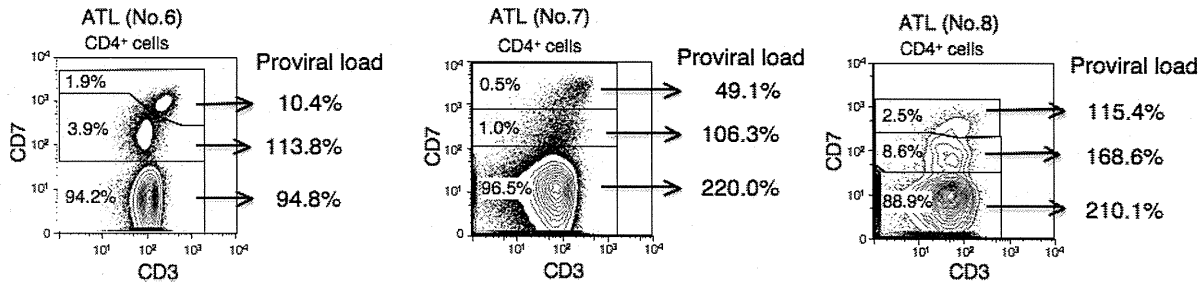


**Fig. 2.** Quantification of the human T-cell leukemia virus type 1 (HTLV-I) proviral load in $CD3^{high}CD7^{high}$, $CD3^{dim}CD7^{dim}$ and $CD3^{dim}CD7^{low}$ subpopulations. Genomic DNA was extracted from the FACS-sorted cells of each subpopulation and subjected to real-time quantitative PCR Representative data of three cases (patients no. 6, 7 and 8) are shown.

subpopulation was a minor but distinct subpopulation. In contrast, the highest cell density was observed in the $CD3^{dim}CD7^{low}$ subpopulation in all acute-type ATL samples except for patient no. 4, from whom the sample was obtained under conditions of well-controlled ATL during chemotherapy. These subpopulations were distinct but the expression pattern of the CD3 *vs* CD7 plot, such as the degree of downregulation of CD3 and CD7, was variable among patients. The proportion of the $CD3^{dim}CD7^{low}$ subpopulation was significantly higher in acute-type ATL $CD4^+$ lymphocytes than in normal controls (Fig. 1C).

**Analysis of the HTLV-I proviral load in $CD3^{high}CD7^{high}$, $CD3^{dim}CD7^{dim}$ and $CD3^{dim}CD7^{low}$ subpopulations.** We next estimated the HTLV-I proviral load by quantitative real-time PCR in each FACS-sorted subpopulation. Representative results from three patients with acute-type ATL (patients no. 6, 7 and 8) are shown in Figure 2. In all patient samples, HTLV-I proviral integration, analyzed by real-time PCR, was detected in all subpopulations. However, the proviral load (%) was significantly higher in $CD3^{dim}CD7^{dim}$ and $CD3^{dim}CD7^{low}$ subpopulations compared with the $CD3^{high}CD7^{high}$ subpopulation. The proviral load of the $CD3^{dim}CD7^{low}$ subpopulation in patients no. 7 and 8 was nearly 200%, indicating integration of two copies of the HTLV-I viral genome and that almost all of the cells were infected with HTLV-I. Similarly, in patient no. 6, the majority of the $CD3^{dim}CD7^{low}$ subpopulation was infected with HTLV-I. A substantial proportion of the $CD3^{dim}CD7^{dim}$ subpopulation was infected with HTLV-I in patients no. 7 and 8, and nearly all the cells in the same subpopulation in patient no. 6 were infected with HTLV-I.

**Differences in the immunophenotype of $CD3^{high}CD7^{high}$, $CD3^{dim}CD7^{dim}$ and $CD3^{dim}CD7^{low}$ subpopulations in patients with acute-type ATL.** To further characterize these three subpopulations, we next examined CCR4 and CD25 expression in each subpopulation. Representative results of a normal control and a patient with acute-type ATL are shown in Figure 3A. The mean fluorescence intensities (MFI) of CD25 and CCR4 of each sub-

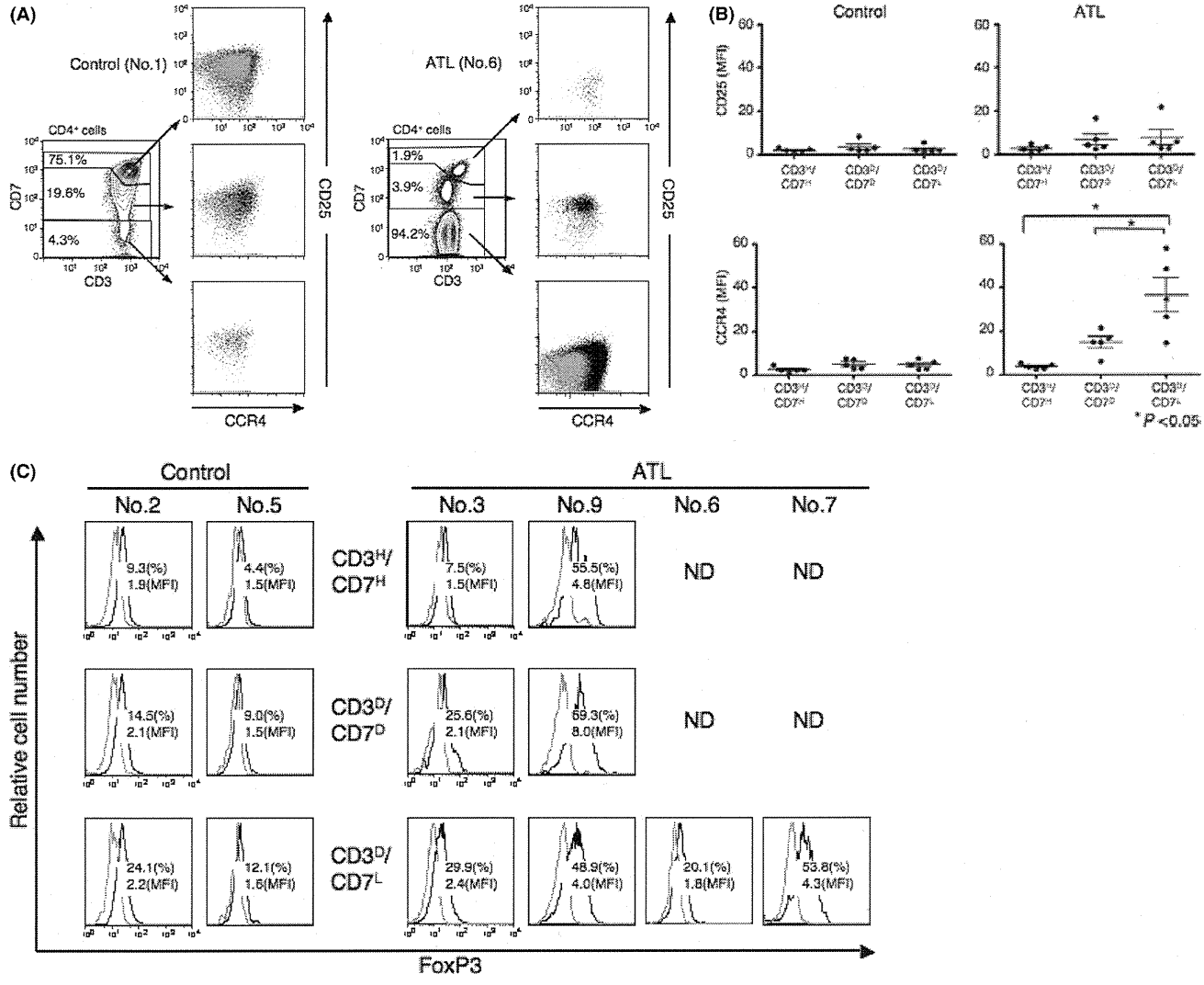


**Fig. 3.** Immunophenotypic analysis in $CD3^{high}CD7^{high}$, $CD3^{dim}CD7^{dim}$ and $CD3^{dim}CD7^{low}$ subpopulations. (A) Expression of CCR4 and CD25 in each subpopulation. Representative FACS data of a normal control (no. 1) and a patient with adult T-cell leukemia (ATL) (no. 6) are shown Gray dots, isotype antibody-stained cells; black dots, specific antibody-stained cells. (B) Mean fluorescence intensity (MFI) of CD25 and CCR4 in each subpopulation from all normal controls and patients with ATL. The MFI is shown in arbitrary units defined as follows: MFI of specific antibody/MFI of isotype antibody. Each dot represents a sample $*P < 005$ by ANOVA. (C) Expression of FoxP3 in each subpopulation. ND, analysis could not be performed in the $CD3^{high}CD7^{high}$ and $CD3^{dim}CD7^{dim}$ subpopulations in patients no. 6 and 7 due to an insufficient number of cells.


doi: 10.1111/j.1349-7006.2010.01833.x

population in all patients with ATL and normal controls are shown in Figure 3B. Both CCR4 and CD25 expression levels were very low and maintained at similar levels throughout all subpopulations in normal control cells and in the $CD3^{high}CD7^{high}$ subpopulation of patients with ATL. In contrast, CCR4 expression was significantly upregulated in the $CD3^{dim}CD7^{dim}$ and $CD3^{dim}CD7^{low}$ subpopulations of patients with ATL compared with the $CD3^{high}CD7^{high}$ subpopulation. The expression of CD25 was also upregulated in these subpopulations but this difference was not significant ($P = 0.36$). The expression of Forkhead box P3 (FoxP3), a master regulator in the development and function of regulatory T (Treg) cells,[14] was also analyzed in some patients. As shown in Figure 3C, FoxP3 expression in the $CD3^{dim}CD7^{low}$ subpopulations was variably upregulated among patients. In addition, in patient no. 9, FoxP3 was upregulated in the $CD3^{high}CD7^{high}$ and $CD3^{dim}CD7^{dim}$ subpopulations.

**Analysis of clonality in the $CD3^{high}CD7^{high}$, $CD3^{dim}CD7^{dim}$ and $CD3^{dim}CD7^{low}$ subpopulations by inverse long PCR.** To further analyze the enrichment of ATL cells in the $CD3^{dim}CD7^{low}$ subpopulation, we estimated clonality in each FACS-sorted subpopulation by inverse long PCR in four patients with acute-type ATL (Fig. 4). An intense band, suggesting a major clone, was detected in the $CD3^{dim}CD7^{low}$ subpopulations in all patients. In the same subpopulation, multiple bands with weak intensity were also observed. As the levels of DNA extracted from the $CD3^{dim}CD7^{low}$ subpopulation were sufficient, we performed duplicate PCR in three patient samples (Fig. 4B–D). Detection of the major bands was consistent, but the presence of the minor bands was variable. In the $CD3^{dim}CD7^{dim}$ subpopulations, bands of the same size as those of the $CD3^{dim}CD7^{low}$ subpopulations were observed, indicating that a distinct population in the $CD3^{dim}CD7^{dim}$ subpopulations belonged to identical clones.

**Clonality in the $CD3^{high}CD7^{high}$, $CD3^{dim}CD7^{dim}$ and $CD3^{dim}CD7^{low}$ subpopulations by flow cytometry-based TCR-Vβ repertoire analysis.** To further confirm clonality and to evaluate the degree of enrichment in each subpopulation, we performed TCR-Vβ repertoire analysis by flow cytometry[15] in three ATL cases. The representative results are shown in Figure 5. In patient no. 3, over 95% of the $CD3^{dim}CD7^{low}$ subpopulation used specific TCR-Vβ (Vβ9) and their proportion was quite low in the $CD3^{high}CD7^{high}$ and $CD3^{dim}CD7^{dim}$ subpopulations. In addition, in the two other cases, over 90% of cells in the $CD3^{dim}CD7^{low}$ subpopulation used the same TCR-Vβ (data not shown). These results indicate that ATL cells are highly purified in the $CD3^{dim}CD7^{low}$ subpopulation.

**Differences in morphology of the $CD3^{high}CD7^{high}$, $CD3^{dim}CD7^{dim}$, and $CD3^{dim}CD7^{low}$ subpopulations in patients with acute-type ATL.** We reviewed the glass-slide specimens of FACS-sorted samples to evaluate the morphology of each subpopulation on the CD3 *vs* CD7 plots. Representative results for two patients (no. 6 and 7) are shown in Figure 6A. In both patients, atypical lymphocytes with notched nuclei and/or basophilic cytoplasm were observed in all three subpopulations. In contrast, abnormal lymphocytes, including cells with multilobulated nuclei (flower cells) were mainly observed in the $CD3^{dim}CD7^{low}$ subpopulation in patient no. 6 (Fig. 6, left) and in the $CD3^{dim}CD7^{dim}$ and $CD3^{dim}CD7^{low}$ subpopulations in patient no. 7 (Fig. 6, right panel).

## Discussion

To investigate the characteristics of ATL cells, the purification of tumor cells is essential. In the present study, we successfully discriminated the $CD3^{dim}CD7^{low}$ subpopulation in $CD4^+$ T cells in the peripheral blood of patients with acute-type ATL by constructing a CD3 *vs* CD7 plot of $CD4^+$ T cells from multi-color FACS (Fig. 1). Previously, Yokote *et al.*[10] reported that $CD3^{low}$ gating facilitated the discrimination of ATL cells by flow cytometry. If we constructed a CD4 *vs* either CD3 or CD7 plot, in which the downregulated cell subpopulation was not clearly separated, then we could not define distinct cell subpopu-

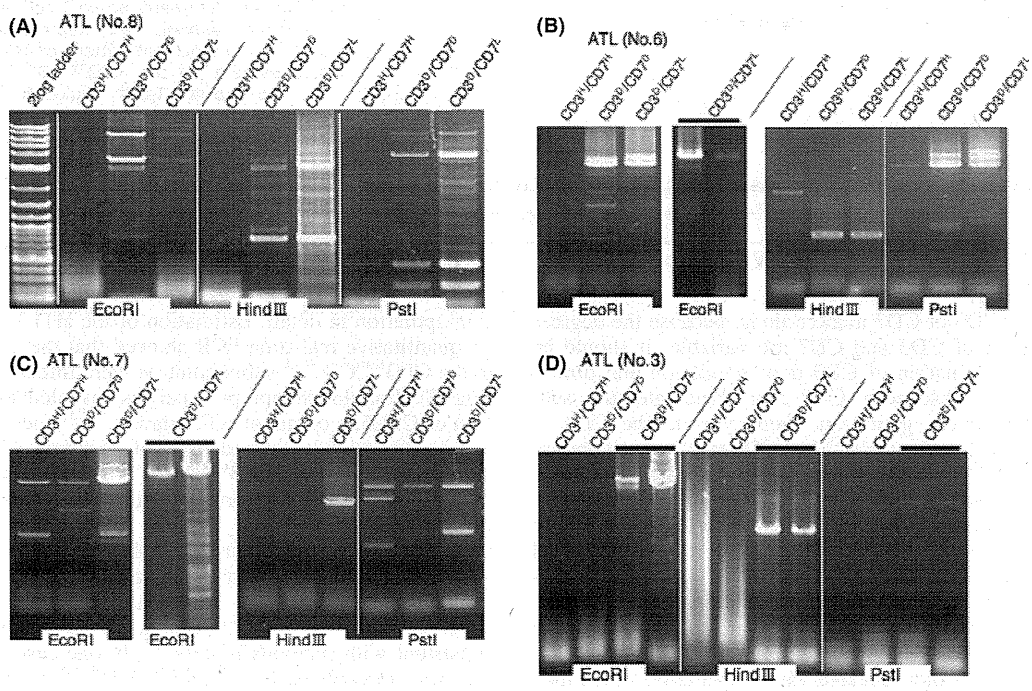


**Fig. 4.** Analysis of clonality in the $CD3^{high}CD7^{high}$, $CD3^{dim}CD7^{dim}$ and $CD3^{dim}CD7^{low}$ subpopulations using inverse long PCR. (A–D) Genomic DNA was extracted from FACS-sorted cells of each subpopulation and subjected to inverse long PCR. Representative data of four cases (patients no. 3, 6, 7 and 8) are shown For the $CD3^{dim}CD7^{low}$ subpopulations of patients no. 3, 6 and 7, PCR was performed in duplicate (black bars). ATL, adult T-cell leukemia.

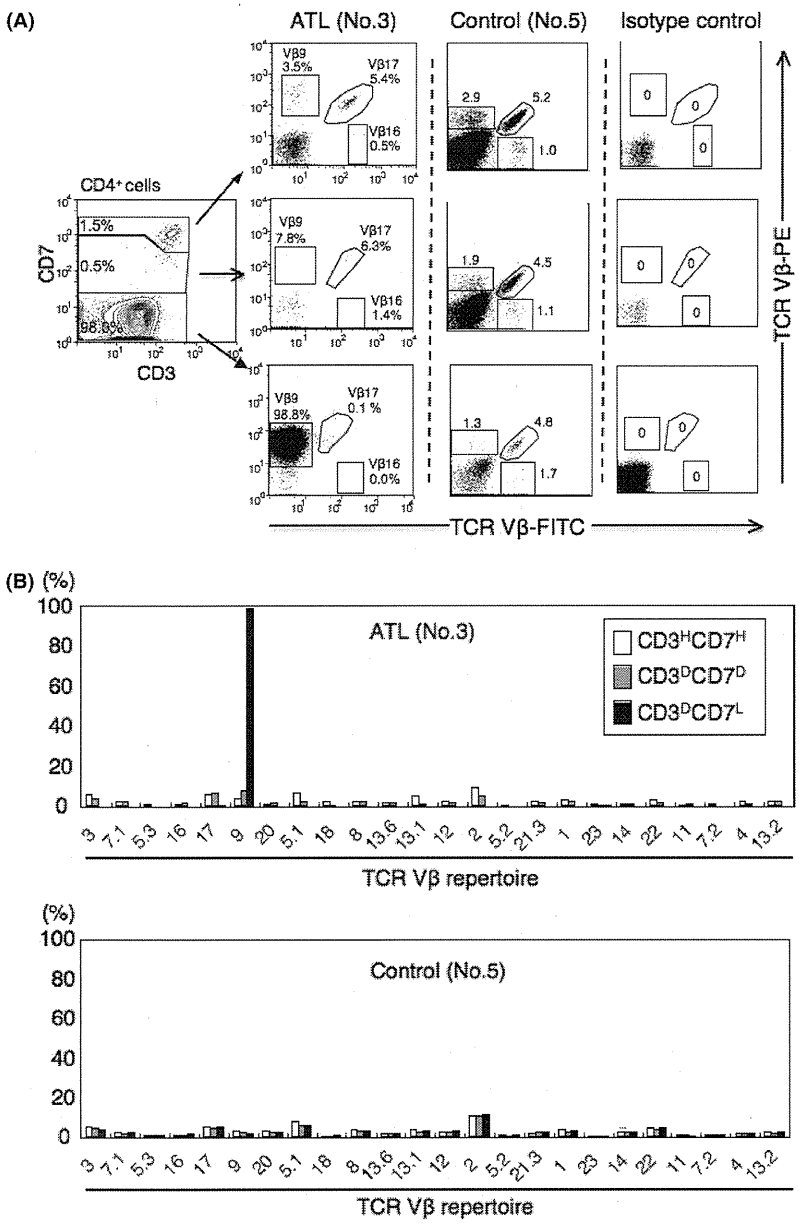


**Fig. 5.** Clonality in the $CD3^{high}CD7^{high}$, $CD3^{dim}CD7^{dim}$ and $CD3^{dim}CD7^{low}$ subpopulations using flow cytometry-based T-cell receptor (TCR)-Vβ repertoire analysis. (A) Representative data are shown A monoclonal pattern of TCR-Vβ9 expression was evident in the $CD3^{dim}CD7^{low}$ subpopulation of the adult T-cell leukemia (ATL) sample. Representative dot plots of 3 of the 24 TCR-Vβ repertoire (Vβ9, 16 and 17) are shown. (B) Bar graph representation of the data from Figure 5A. The percentages of cells positive for each TCR-Vβ repertoire in the $CD3^{high}CD7^{high}$, $CD3^{dim}CD7^{dim}$ and $CD3^{dim}CD7^{low}$ subpopulations. White bar, $CD3^{high}CD7^{high}$; gray bar, $CD3^{dim}CD7^{dim}$; black bar, $CD3^{dim}CD7^{low}$.

lations using the CD3 or CD7 marker alone, because the degrees of downregulation of CD3 and CD7 are variable. It should be noted that the combination of CD3 downregulation and diminished expression or absence of CD7 clearly indicates this subpopulation. In addition, gating-out monocytes in the CD4 *vs* CD14 plot is important for the CD3 *vs* CD7 plot because monocytes were CD3/CD7 dull-positive based on the nonspecific binding of the antibody.

A substantial subpopulation of T cells has been reported to be CD7-deficient under physiological[16,17] and certain pathological conditions, including autoimmune disorders and viral infection.[18–22] Consistent with these reports, the present study indicated that the proportion of $CD4^+CD7^-$ T cells in the peripheral blood of healthy adults is up to 10% (Fig. 1B,C). In ATL samples, the CD3 *vs* CD7 plot revealed various patterns, which may reflect the differences in clinical characteristics of each patient; however, the $CD3^{dim}CD7^{low}$ subpopulation, which was a minor population in the normal controls, was prominent in all ATL samples (Fig. 1B,C). These results prompted us to study this subpopulation in detail. Estimation of the HTLV-I proviral load by quantitative real-time PCR showed that the majority of cells in the $CD3^{dim}CD7^{low}$ subpopulation were infected with HTLV-I (Fig. 2). Immunophenotypic analysis revealed that the expression of CD25, a common ATL marker,[9,23] and CCR4, reported to be expressed in around 90% of cases of ATL,[24,25] were upregulated in the $CD3^{dim}CD7^{low}$ subpopulations of ATL samples in contrast to normal controls in which both markers were weakly expressed in the equivalent subpopulation (Fig. 3A,B). As several studies indicated that ATL cells originate from $CD4^+CD25^+FoxP3^+$ Treg cells,[26] we next analyzed FoxP3 expression in each subpopulation. In the $CD3^{dim}CD7^{low}$ subpopulation, the FoxP3 expression levels were variable, consistent with previous reports.[27] In one case, FoxP3 expression was upregulated in the $CD3^{high}CD7^{high}$ and $CD3^{dim}CD7^{dim}$ subpopulations suggesting that they were normal Treg cells.

The analysis of clonality is extremely important for determining whether cells are transformed and Southern blot analysis is usually used to confirm clonality. However, in the present study,


doi: 10.1111/j.1349-7006.2010.01833.x

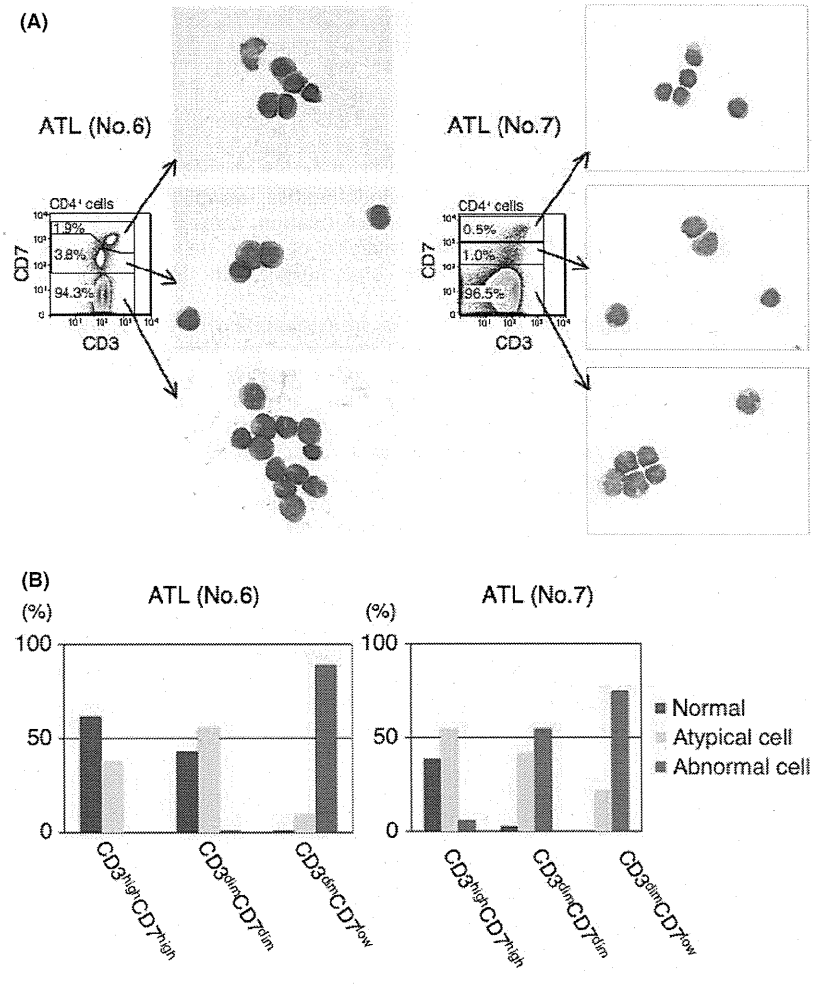


**Fig. 6.** Morphology of the $CD3^{high}CD7^{high}$, $CD3^{dim}CD7^{dim}$ and $CD3^{dim}CD7^{low}$ subpopulations in two representative adult T-cell leukemia (ATL) samples (patients no. 6 and 7). (A) May–Giemsa staining of FACS-sorted cells from each subpopulation from two patients with acute-type ATL. Top, $CD3^{high}CD7^{high}$ subpopulation; middle, $CD3^{dim}CD7^{dim}$ subpopulation; bottom, $CD3^{dim}CD7^{low}$ subpopulation. (B) Percentages of cells with different morphology in each subpopulation. Normal, lymphocytes with normal morphology; atypical, lymphocytes with notched nuclei and basophilic cytoplasm; abnormal, lymphocytes with convoluted, deeply indented or multilobulated flower cells.

the cell number following cell sorting was not sufficient for Southern blotting, and thus inverse long PCR for clonality analysis of HTLV-I-infected cells was used.[25] Studies of four ATL samples revealed clonal expansion of ATL cells in the $CD3^{dim}CD7^{low}$ subpopulations, although minor clones may exist in the population (Fig. 4). When PCR was performed in duplicate, we found that the major bands were consistently detected in all cases. However, the detection of multiple minor bands was not consistent. As reported previously, the inverse long PCR method stochastically amplifies the template originating from small clones.[28,29] The minor bands observed in the present study will contain small clones. However, the presence of non-specific bands cannot be eliminated.

The inverse long PCR method is commonly used for clonality analysis; however, it cannot quantify the size of major/minor clones and the degree of enrichment in each subpopulation. Therefore, we tested the FACS-based TCR-Vβ repertoire analysis combined with our multi-color FACS system (Fig. 5). In ATL patient no. 3, almost all cells in the $CD3^{dim}CD7^{low}$ subpopulations were clonal cells with TCR-Vβ9. Inverse long PCR analysis in the same patient showed multiple minor bands in the $CD3^{dim}CD7^{low}$ subpopulations (Fig. 4D). These results did not conflict with those of the TCR-Vβ repertoire analysis, as the inverse long PCR method is a more sensitive method for detecting small clones compared with flow cytometry. Taken together, the series of analyses in the present study indicated that the $CD3^{dim}CD7^{low}$ subpopulations consist of highly purified ATL cells in patients with acute-type ATL.

A substantial proportion of cells in the $CD3^{dim}CD7^{dim}$ subpopulation consisted of morphologically abnormal lymphocytes (Fig. 6) that exhibited upregulation of CD25 and CCR4 expression (Fig. 3A,B). Using the inverse long PCR method, a similar band pattern between $CD3^{dim}CD7^{dim}$ and $CD3^{dim}CD7^{low}$ subpopulations was observed in patients no. 6 and 8, suggesting that these cells belonged to the same clone (Fig. 4A,B). However, not all of the cells in this subpopulation were infected with HTLV-I because the HTLV-I proviral load was less than that of the $CD3^{dim}CD7^{low}$ subpopulation (Fig. 2). Thus, at least a small number of the $CD3^{dim}CD7^{dim}$ cells were expected to be ATL cells. Those cells observed in the $CD3^{dim}CD7^{dim}$ subpopulation that were phenotypically different from the $CD3^{dim}CD7^{low}$ subpopulations were of particular interest. We detected a band of the same size on inverse long PCR in the $CD3^{dim}CD7^{dim}$ subpopulations as in the $CD3^{dim}CD7^{low}$ subpopulation. This may have been because the two subpopulations originated from the same clone that evolved from a $CD3^{dim}CD7^{dim}$ to a $CD3^{dim}CD7^{low}$ phenotype. Further studies are required to determine the characteristics of the $CD3^{dim}CD7^{dim}$ subpopulation in greater detail.

The results of the present study indicated that HTLV-I-infected cells distribute from a $CD7^{high}$ to a $CD7^{low}$ subpopulation, although the proportion of HTLV-I-infected cells was remarkably low in the $CD3^{high}CD7^{high}$ subpopulation (Fig. 2). A considerable proportion of cells in the $CD3^{high}CD7^{high}$ subpopulation consisted of morphologically atypical lymphocytes (Fig. 6), but the CD25 and CCR4 levels were not upregulated

(Fig. 3A,B). When analyzing the pattern of the inverse long PCR of the $CD3^{high}CD7^{high}$ subpopulations, we observed a difference from those of the $CD3^{dim}CD7^{dim}$ and $CD3^{dim}CD7^{low}$ subpopulations (Fig. 4). In patients no. 6 (Fig. 4B) and 7 (Fig. 4C), the band detected in the $CD3^{high}CD7^{high}$ subpopulation may represent an expanded clone that was not transformed. Most likely, these cells do not represent ATL cells, but oligoclonal HTLV-I-infected lymphocytes. Previous studies indicated that HTLV-I-infected cells undergo transformation through multi-step oncogenesis.[30] A detailed analysis of these three subpopulations may therefore provide some insight into the oncogenesis of HTLV-I-infected cells.

Accurate determination of ATL cells in peripheral blood is critical for estimating the response to chemotherapy. However, as discussed above, morphological studies (Fig. 6) have limitations in their ability to discriminate ATL from non-ATL cells.[31,32]. Recently, hematopoietic stem cell transplantation has been explored as a promising treatment to overcome the poor prognosis of this most incurable lymphoid malignancy,[33,34] and monitoring minimal residual disease following hematopoietic stem cell transplantation is more important. Our method of analyzing ATL cells may be particularly useful for monitoring minimal residual disease. Although the $CD3^{dim}CD7^{dim}$ subpopulation in our analysis may have included some ATL cells, this is a minor population in the peripheral blood of patients with acute-type ATL, and it is sufficient for practical use to monitor the $CD3^{dim}CD7^{low}$ subpopulation. Another possible use of our procedure is for the definitive classification of ATL subtypes according to Shimoyama's criteria.[8] A proportion of abnormal lymphocytes in peripheral blood comprise part of the criteria for ATL-subtype classification but it is sometimes confusing. Our multi-color FACS system may clearly quantify this proportion.

In conclusion, we have constructed a multi-color FACS system to purify ATL cells in the peripheral blood of patients with acute-type ATL. This system may be useful for precisely monitoring the disease during chemotherapy, detecting minimal residual disease and analyzing ATL cells. This system may be of great benefit in investigating oncogenesis in HTLV-I-infected cells.

## Acknowledgments

The authors thank Dr. Toshiki Watanabe, Dr. Kazumi Nakano and Dr. Tadanori Yamochi (The University of Tokyo) for providing the TL-Om1 cell line and plasmid containing the HTLV-I genome, which were used as standards for quantification of the proviral load. We are also grateful for their substantial technical assistance. We thank Dr. Naofumi Mastsuno (The University of Tokyo) for providing technical assistance regarding multi-color flow cytometry. We are grateful to the hospital staff that have made a commitment to providing high quality care for all of our patients. This study was supported by the Ministry of Education, Culture, Sports, Science and Technology and the Ministry of Health, Labor, and Welfare of Japan.

## Disclosure Statement

The authors declare no financial conflicts of interest.

## References

1 Yoshida M, Miyoshi I, Hinuma Y. Isolation and characterization of retrovirus from cell lines of human adult T-cell leukemia and its implication in the disease. *Proc Natl Acad Sci U S A* 1982; **79** (6): 2031–5.
2 Matsuoka M. Human T-cell leukemia virus type I (HTLV-I) infection and the onset of adult T-cell leukemia (ATL). *Retrovirology* 2005; **2**: 27.
3 Nicot C. Current views in HTLV-I-associated adult T-cell leukemia/lymphoma. *Am J Hematol* 2005; **78** (3): 232–9.
4 Ginaldi L, Matutes E, Farahat N, De Martinis M, Morilla R, Catovsky D. Differential expression of CD3 and CD7 in T-cell malignancies: a quantitative study by flow cytometry. *Br J Haematol* 1996; **93** (4): 921–7.
5 Campana D, Coustan-Smith E. Minimal residual disease studies by flow cytometry in acute leukemia. *Acta Haematol* 2004; **112** (1–2): 8–15.
6 Craig FE, Foon KA. Flow cytometric immunophenotyping for hematologic neoplasms. *Blood* 2008; **111** (8): 3941–67.
7 Akl H, Badran B, Dobirta G *et al.* Progressive loss of CD3 expression after HTLV-I infection results from chromatin remodeling affecting all the CD3 genes and persists despite early viral genes silencing. *Virol J* 2007; **4**: 85.
8 Shimoyama M. Diagnostic criteria and classification of clinical subtypes of adult T-cell leukaemia-lymphoma. A report from the Lymphoma Study Group (1984–87). *Br J Haematol* 1991; **79** (3): 428–37.
9 Tsukasaki K, Hermine O, Bazarbachi A *et al.* Definition, prognostic factors, treatment, and response criteria of adult T-cell leukemia-lymphoma: a proposal from an international consensus meeting. *J Clin Oncol* 2009; **27** (3): 453–9.
10 Yokote T, Akioka T, Oka S *et al.* Flow cytometric immunophenotyping of adult T-cell leukemia/lymphoma using CD3 gating. *Am J Clin Pathol* 2005; **124** (2): 199–204.
11 Yamada Y, Tomonaga M, Fukuda H *et al.* A new G-CSF-supported combination chemotherapy, LSG15, for adult T-cell leukaemia-lymphoma: Japan Clinical Oncology Group Study 9303. *Br J Haematol* 2001; **113** (2): 375–82.
12 Roncador G, Brown PJ, Maestre L *et al.* Analysis of FOXP3 protein expression in human CD4+CD25+ regulatory T cells at the single-cell level. *Eur J Immunol* 2005; **35** (6): 1681–91.
13 Iwanaga M, Watanabe T, Utsunomiya A *et al.* Human T-cell leukemia virus type I (HTLV-I) proviral load and disease progression in asymptomatic HTLV-I carriers: a nationwide prospective study in Japan. *Blood* 2010; **116** (8): 1211–19.
14 Sakaguchi S. Naturally arising Foxp3-expressing CD25+CD4+ regulatory T cells in immunological tolerance to self and non-self. *Nat Immunol.* 2005; **6** (4): 345–52.
15 Morice WG, Kimlinger T, Katzmann JA *et al.* Flow cytometric assessment of TCR-Vbeta expression in the evaluation of peripheral blood involvement by T-cell lymphoproliferative disorders: a comparison with conventional T-cell immunophenotyping and molecular genetic techniques. *Am J Clin Pathol* 2004; **121** (3): 373–83.
16 Reinhold U, Abken H. CD4+ CD7- T cells: a separate subpopulation of memory T cells? *J Clin Immunol* 1997; **17** (4): 265–71.
17 Reinhold U, Abken H, Kukel S *et al.* CD7- T cells represent a subset of normal human blood lymphocytes. *J Immunol* 1993; **150** (5): 2081–9.
18 Aandahl EM, Quigley MF, Moretto WJ *et al.* Expansion of CD7(low) and CD7(negative) CD8 T-cell effector subsets in HIV-1 infection: correlation with antigenic load and reversion by antiretroviral treatment. *Blood* 2004; **104** (12): 3672–8.
19 Autran B, Legac E, Blanc C, Debre P. A Th0/Th2-like function of CD4 + CD7- T helper cells from normal donors and HIV-infected patients. *J Immunol* 1995; **154** (3): 1408–17.
20 Legac E, Autran B, Merle-Beral H, Katlama C, Debre P. CD4+CD7-CD57+ T cells: a new T-lymphocyte subset expanded during human immunodeficiency virus infection. *Blood* 1992; **79** (7): 1746–53.
21 Schmidt D, Goronzy JJ, Weyand CM. CD4+ CD7- CD28- T cells are expanded in rheumatoid arthritis and are characterized by autoreactivity. *J Clin Invest* 1996; **97** (9): 2027–37.
22 Willard-Gallo KE, Van de Keere F, Kettmann R. A specific defect in CD3 gamma-chain gene transcription results in loss of T-cell receptor/CD3 expression late after human immunodeficiency virus infection of a CD4+ T-cell line. *Proc Natl Acad Sci U S A* 1990; **87** (17): 6713–17.
23 Matsuoka M, Jeang KT. Human T-cell leukaemia virus type 1 (HTLV-I) infectivity and cellular transformation. *Nat Rev Cancer* 2007; **7** (4): 270–80.
24 Ishida T, Utsunomiya A, Iida S *et al.* Clinical significance of CCR4 expression in adult T-cell leukemia/lymphoma: its close association with skin involvement and unfavorable outcome. *Clin Cancer Res* 2003; **9** (10 Pt 1): 3625–34.
25 Yoshie O, Fujisawa R, Nakayama T *et al.* Frequent expression of CCR4 in adult T-cell leukemia and human T-cell leukemia virus type 1-transformed T cells. *Blood* 2002; **99** (5): 1505–11.
26 Yano H, Ishida T, Inagaki A *et al.* Regulatory T-cell function of adult T-cell leukemia/lymphoma cells. *Int J Cancer* 2007; **120** (9): 2052–7.
27 Abe M, Uchihashi K, Kazuto T *et al.* Foxp3 expression on normal and leukemic CD4+CD25+ T cells implicated in human T-cell leukemia virus type-1 is inconsistent with Treg cells. *Eur J Haematol* 2008; **81** (3): 209–17.



doi: 10.1111/j.1349-7006.2010.01833.x

28 Tanaka G, Okayama A, Watanabe T *et al.* The clonal expansion of human T lymphotropic virus type 1-infected T cells: a comparison between seroconverters and long-term carriers. *J Infect Dis* 2005; **191** (7): 1140–7.
29 Cavrois M, Wain-Hobson S, Wattel E. Stochastic events in the amplification of HTLV-I integration sites by linker-mediated PCR. *Res Virol* 1995; **146** (3): 179–84.
30 Verdonck K, Gonzalez E, Van Dooren S, Vandamme AM, Vanham G, Gotuzzo E. Human T-lymphotropic virus 1: recent knowledge about an ancient infection. *Lancet Infect Dis* 2007; **7** (4): 266–81.
31 Sakamoto Y, Kawachi Y, Uchida T *et al.* Adult T-cell leukaemia/lymphoma featuring a large granular lymphocyte leukaemia morphologically. *Br J Haematol* 1994; **86** (2): 383–5.
32 Tsukasaki K, Imaizumi Y, Tawara M *et al.* Diversity of leukaemic cell morphology in ATL correlates with prognostic factors, aberrant immunophenotype and defective HTLV-I genotype. *Br J Haematol* 1999; **105** (2): 369–75.
33 Okamura J, Utsunomiya A, Tanosaki R *et al.* Allogeneic stem-cell transplantation with reduced conditioning intensity as a novel immunotherapy and antiviral therapy for adult T-cell leukemia/lymphoma. *Blood* 2005; **105** (10): 4143–5.
34 Utsunomiya A, Miyazaki Y, Takatsuka Y *et al.* Improved outcome of adult T-cell leukemia/lymphoma with allogeneic hematopoietic stem cell transplantation. *Bone Marrow Transplant.* 2001; **27** (1): 15–20.

Stem Cell Rev and Rep (2011) 7:958–968
DOI 10.1007/s12015-011-9249-3

# Variation in Mesodermal and Hematopoietic Potential of Adult Skin-derived Induced Pluripotent Stem Cell Lines in Mice

**Tomoko Inoue · Kasem Kulkeaw · Satoko Okayama · Kenzaburo Tani · Daisuke Sugiyama**

Published online: 19 March 2011


**Abstract** Induced pluripotent stem cells (iPSCs) are a promising tool for regenerative medicine. Use of iPSC lines for future hematotherapy will require examination of their hematopoietic potential. Adult skin fibroblast somatic cells constitute a source of iPSCs that can be accessed clinically without ethical issues. Here, we used different methods to compare mesodermal and hematopoietic potential by embryoid body formation of five iPSC lines established from adult mouse tail-tip fibroblasts (TTFs). We observed variation in proliferation and in expression of genes (*Brachyury, Tbx1, Gata1, Klf1, Csf1r*) and proteins (Flk1, Ter119 and CD45) among TTF-derived lines. 256H18 iPSCs showed highest proliferation and most efficient differentiation into mesodermal and hematopoietic cells, while expression levels of the pluripotency genes *Oct3/4, Sox2, Klf4* and *Nanog* were lowest among lines analyzed. By contrast, the 212B2 line, transduced with *c-Myc*, showed lowest proliferation and differentiation potential, although expression levels of *Oct3/4, Sox2* and *Klf4* were highest. Overall, we find that mesodermal and hematopoietic potential varies among iPSCs from an identical tissue source and that *c-Myc* expression likely underlies these differences.

**Electronic supplementary material** The online version of this article (doi:10.1007/s12015-011-9249-3) contains supplementary material, which is available to authorized users.

T. Inoue · K. Kulkeaw · S. Okayama · D. Sugiyama (✉)
Department of Hematopoietic Stem Cells, SSP Stem Cell Unit,
Kyushu University Faculty of Medical Sciences,
Station for Collaborative Research 1 4F,
3-1-1 Maidashi, Higashi-Ku, Fukuoka 812–8582, Japan
e-mail: ds-mons@yb3.so-net.ne.jp

T. Inoue · K. Tani
Department of Molecular Genetics,
Medical Institute of Bioregulation, Kyushu University,
Fukuoka 812–8582, Japan

**Keywords** Induced pluripotent stem cells · Tail-tip fibroblasts · Embryoid body · Mesodermal induction · Hematopoietic potential

## Introduction

Hematopoietic stem cells (HSCs) are already in use for transplantation therapy for hematological diseases. However, problems associated with HSC transplantation remain, such as a shortage of donors or immunoreactivity caused by HLA mismatching (rejection and graft versus host disease (GVHD)). To overcome these issues, induced pluripotent stem cells (iPSCs) could serve to generate autologous HSCs without the need for a donor. iPSCs have been established from various somatic cells by forced expression of defined factors [1, 2]. These cells display properties similar to embryonic stem cells (ESCs) in terms of differentiation capacity into various cell types, teratoma formation in immuno-deficient mice, and generation of chimeric mice with germ line transmission [3]. Therefore, iPSC technology could enable us to generate cells for clinical purposes without an embryonic source or a donor [4, 5]. Generally, *Oct3/4*, *Sox2*, *Klf4*, and *c-Myc* are retrovirally transduced into somatic cells to initiate reprogramming and establish iPSC lines. Since both expression of the *c-Myc* oncogene and retroviral infection are associated with malignancy, investigators have devised reprogramming protocols lacking *c-Myc* transduction [6] or avoiding use of non-integrated viral vectors [7] or plasmids [8] for gene delivery. Various novel approaches, including combining transcription factors and reporters, have been employed to reprogram various types of somatic cells, such as mouse embryonic fibroblasts (MEFs), adult fibroblasts, pancreatic β-cells, hepatocytes, gastric epithelial cells, B cells, and $CD34^+$ cord blood cells

[9–11]. Among these cell types, adult skin fibroblasts are a desirable potential source of somatic cells, since they can be clinically accessed without ethical problems. To help devise future clinical transplantation therapies, it is necessary to determine which iPSCs derived from tail-tip fibroblasts (TTFs) (adult skin fibroblasts in mice) are most fit to generate HSCs.

Previously, we reported variation in hematopoietic potential among several iPSC lines, regardless of the source of somatic cells [12]. This observation suggested that variation in hematopoietic potential could occur among TTF-derived iPSCs. To address this issue, we analyzed mesodermal and hematopoietic potential in five TTF-derived iPSC lines established using different transcription factors (*Oct3/4, Sox2* and *Klf4* with or without *c-Myc*) or reporter genes (*DsRed* or *GFP*). We demonstrate that both mesodermal and hematopoietic cell number and expression of mesoderm and hematopoietic cell differentiation markers varies among the five lines. Interestingly, 212B2 iPSCs, the only line created via *c-Myc* transduction, exhibited lower capacity to differentiate into mesodermal and hematopoietic cells compared than did the other four iPSCs.

## Materials and Methods

### iPSCs Maintenance

We used the five lines of tail-tip fibroblast (TTF)-derived iPSCs, such as 256H13, 256H18, 212B2, 212D1 and 335D1, which were kindly provided by Dr. Shinya Yamanaka (Kyoto University). These iPSCs were established by "separate method" as previously described [6]. Briefly, pMX-Oct3/4, pMX-Klf4, pMX-Sox2, and/or pMX-c-Myc plasmids were separately transfected into separate dishes of Plat-E cells using Fugene 6 reagent (Roche Applied Science, Indianapolis, IN). Twenty-four hours after transfection, the medium was replaced with serum-containing DMEM. After 24 h, each virus-containing supernatant was mixed and used for retroviral infection. Concerning iPSCs generation, TTFs were isolated from adult Nanog-GFP-IRES-Puro$^r$ reporter mice or adult DsRed-transgenic mice. For the four-factor transduction, retrovirus-containing supernatants for *Klf4*, *c-Myc*, *Oct3/4*, *Sox2* and *DsRed*, were mixed with the ratio of 1:1:1:1:4. When the fibroblasts were transduced with the three factors, retrovirus-containing supernatants for *Klf4*, *Oct3/4*, *Sox2*, *DsRed* and Mock were mixed with the ratio of 1:1:1:1:4. For transfection, TTFs were seeded at $8.0\times10^5$ cells in 100-mm dish, without feeder cells. TTFs were incubated in the virus/polybrene-containing supernatants for 24 h. Four days after transduction, TTFs transduced with the three factors were reseeded at $3.5\times10^5$ cells per 100-mm dish with SNL feeder cells and cultured with ES medium containing DMEM, 15% FBS, 0.1 mM non essential amino acid, 0.1 mM 2-mercaptoethanol (2-ME) and 1000U/ml mouse leukemia inhibitory factor (LIF). TTFs transduced with the four factors were reseeded at $0.5\times10^5$ cells per 100-mm dish with feeder cells. Thirty to forty days after transduction, the colonies were selected for expansion. Drug selection with puromycin (1.5 μg/ml) was done for 212B2, 212D1 and 335D1 iPSCs. 256H13 and 256H18 iPSC lines were established without drug selection [6]. Twenty to thirty percent efficiency was achieved in transfection of all five iPSC lines.

We firstly expanded these iPSC lines with mitomycin-C (MMC)-treated mouse embryonic fibroblasts (MEFs) in StemMedium (DS Pharma Biomedical, Hyogo, Japan) containing 0.1 mM 2-ME (Nacalai Tesque, Inc., Kyoto, Japan) and 1000 U/ml mouse LIF (prepared in Dr. Minetaro Ogawa's Laboratory). The passage number (P) for each line used in this study was as follows; 256H13 (P.6-P.9), 256H18 (P.8-P.10), 212B2 (P.9), 212D1 (P.6), and 335D1 (P.8-P.10).

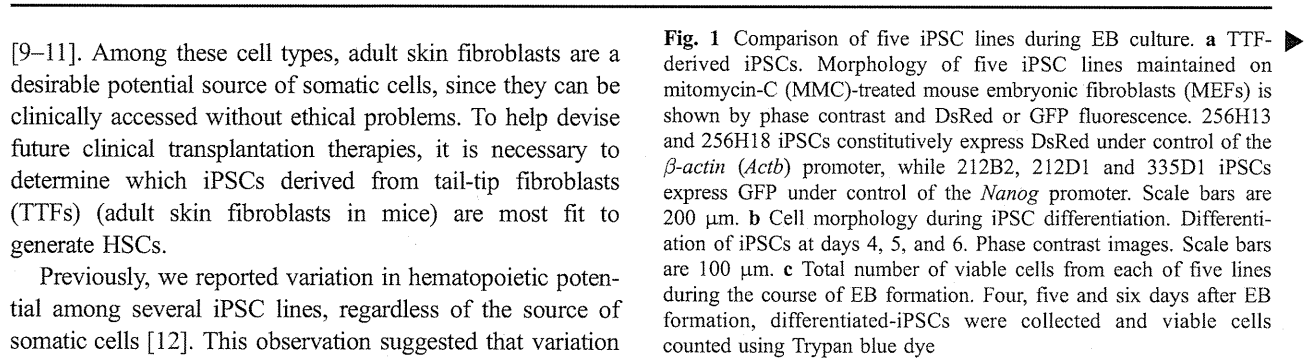

**Fig. 1** Comparison of five iPSC lines during EB culture. **a** TTF-derived iPSCs. Morphology of five iPSC lines maintained on mitomycin-C (MMC)-treated mouse embryonic fibroblasts (MEFs) is shown by phase contrast and DsRed or GFP fluorescence. 256H13 and 256H18 iPSCs constitutively express DsRed under control of the *β-actin* (*Actb*) promoter, while 212B2, 212D1 and 335D1 iPSCs express GFP under control of the *Nanog* promoter. Scale bars are 200 μm. **b** Cell morphology during iPSC differentiation. Differentiation of iPSCs at days 4, 5, and 6. Phase contrast images. Scale bars are 100 μm. **c** Total number of viable cells from each of five lines during the course of EB formation. Four, five and six days after EB formation, differentiated-iPSCs were collected and viable cells counted using Trypan blue dye

### Embryoid Body (EB) Formation

Before EB formation, iPSCs were separated from feeder cells by 0.5-hour incubation to eliminate the attached MEF cells. Then, iPSCs expressing stage-specific embryonic antigen-1 (SSEA-1) were purified by magnetic cell separation (MACS, Miltenyi Biotec, Auburn, CA). iPSCs ($6\times10^4$ cells) were cultured in 3 ml of EB medium, which contains Iscove's Modified Dulbecco's Medium (IMDM, SIGMA-ALDRICH, St. Louis, MO) containing 15% FBS (a pre-selected batch showing the highest efficiency in inducing hematopoietic cells), 2 mM L-glutamine (SIGMA-ALDRICH), 0.0026% (vol/vol) monothioglycerol (MTG; Wako Pure Chemical Industries, Osaka, Japan), 50 μg/ml L-ascorbic acid (Wako Pure Chemical Industries), 10 U/ml penicillin, and 10 μg/ml streptomycin (SIGMA-ALDRICH).

For mesodermal cell differentiation, no cytokine was added in the EB medium. Petri dishes (60-mm in diameter, Kord-Valmark™, Ontario, Canada) were used to generate EBs. On culture days 4, 5, and 6, cells were collected by gentle pipetting, washed once in PBS, and then incubated in

a

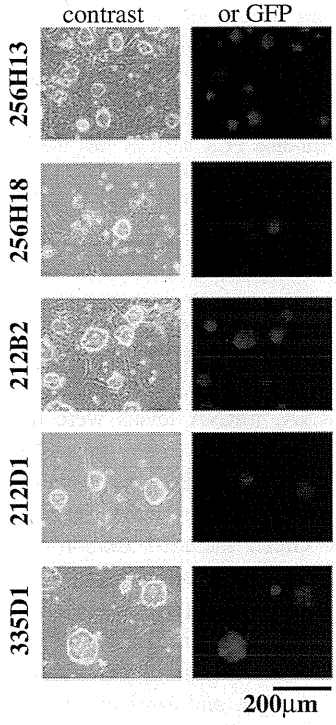


| iPSC line | Transduced genes | Reporter gene | Transduction method | Viral vector | Genetic selection |
|---|---|---|---|---|---|
| iPS-TTF-FB/DsRed-256H13 | Oct3/4, Klf4, Sox2 | Actb-DsRed | Retrovirus | pMX-Oct3/4 pMX-Klf4 pMx-Sox2 | w/o |
| iPS-TTF-FB/DsRed-256H18 | Oct3/4, Klf4, Sox2 | Actb-DsRed | Retrovirus | pMX-Oct3/4 pMX-Klf4 pMX-Sox2 | w/o |
| iPS-TTF-FB/Ng-212B2 | Oct3/4, Klf4, Sox2, c-Myc | Nanog-GFP | Retrovirus | pMX-Oct3/4 pMX-Klf4 pMX-Sox2 pMX-c-Myc | Nanog |
| iPS-TTF-FB/Ng-212D1 | Oct3/4, Klf4, Sox2 | Nanog-GFP | Retrovirus | pMX-Oct3/4 pMX-Klf4 pMX-Sox2 | Nanog |
| iPS-TTF-FB/Ng-335D1 | Oct3/4, Klf4, Sox2 | Nanog-GFP | Retrovirus | pMX-Oct3/4 pMX-Klf4 pMX-Sox2 | Nanog |

b

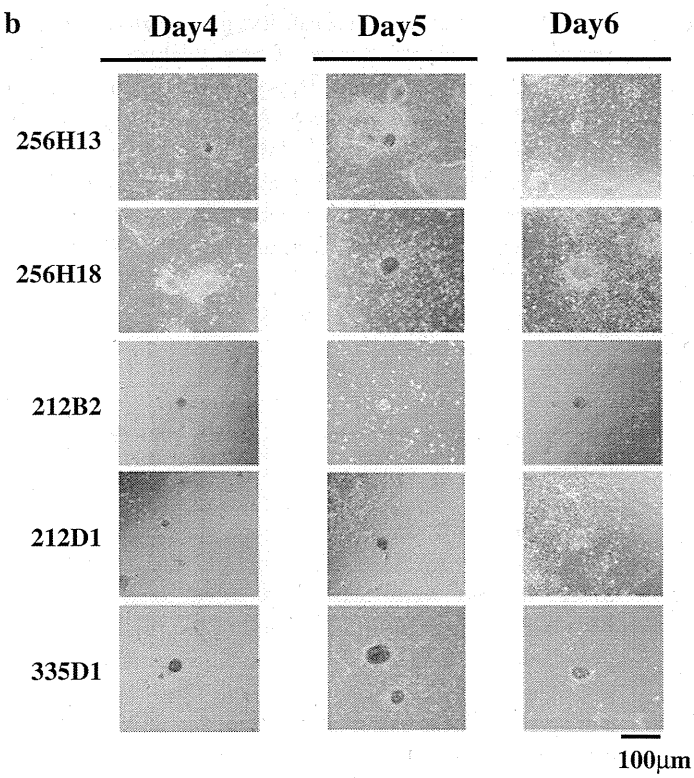


c

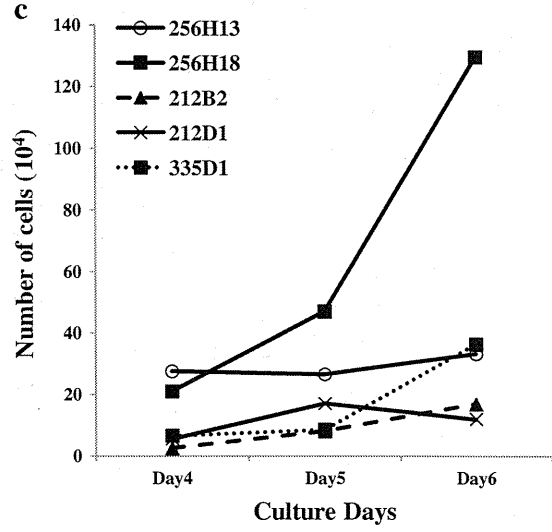

Cell Dissociation Buffer (Life Technologies, Carlsbad, CA) at 37°C for 30 min. An equal volume of medium containing 10% FBS was added and mixed gently by pipetting, and the cell suspension was passed through a 40-μm nylon mesh. The number of living cells was determined by staining with 0.4% Trypan blue (Life Technologies). For hematopoietic cell differentiation, SCF (stem cell factor), IL (interleukin)-3, EPO (erythropoietin), IL-6 and G-CSF (granulocyte colony-stimulating factor) were added in the EB medium. Petri dishes were used to generate EBs. On culture days 9, cells were collected and counted as mentioned above.

### Flow Cytometry

To analyze mesodermal cells from iPSCs, cells cultured for 4, 5, and 6 days were collected as mentioned in 'EB formation' and stained with an APC-conjugated anti-CD324 (E-cadherin) antibody (Ab) (Alexa Fluor®647, eBioscience, San Diego, CA), a Pacific Blue™ -conjugated anti-mouse Flk1 (VEGFR2) Ab (BioLegend, San Diego, CA), a biotin-conjugated anti-mouse CD140α (PDGFRα) Ab (eBioscience) and an APC-Cy7-conjugated streptavidin (BD Biosciences, San Jose, CA). Biotin-conjugated antibody was used as a primary antibody and fluorescence-conjugated streptavidin was used as a secondary reagent, respectively. E-cadherin$^-$/Flk1$^+$ cells were defined as lateral mesodermal cells and E-cadherin$^-$/PDGFRα$^+$ cells as paraxial mesodermal cells, respectively.

To analyze hematopoietic cells from iPSCs, cells cultured for 9 days were collected as mentioned in 'EB formation' section and stained with an APC-Cy7-conjugated anti-mouse Ter119 Ab (eBioscience), a PB-conjugated anti-mouse CD45 Ab (BioLegend), an APC-conjugated anti-mouse F4/80 (BioLegend), a biotin-conjugated anti-mouse Gr-1 Ab (eBioscience) and PE-Cy7-conjugated streptavidin (BD Biosciences). For Mac1 Ab, a PE-conjugated anti-mouse Mac1 Ab (BioLegend) was used for GFP-expressing iPSCs (212B2, 212D1, and 335D1). And a biotin-conjugated anti-mouse Mac1 Ab (eBioscience) and a PE-Cy7-conjugated streptavidin were used for DsRed-expressing iPSCs, respectively. Biotin-conjugated antibody was used as a primary antibody and fluorescence-conjugated streptavidin was used as a secondary reagent, respectively. Ter119 positive cells were defined as erythroid cells, CD45 positive cell as leukocytes, Mac1$^+$/F4/80$^+$ cells as macrophages and Gr-1$^+$/F4/80$^-$ cells as granulocytes, respectively.

To stain dead cells, propidium iodide (PI, Life Technologies, Eugene, Oregon) was used for GFP-expressing iPSCs, and TO-PRO®-1 iodide (Life Technologies) was used for DsRed-expressing iPSCs. Cells were analyzed using a FACS Aria cell sorter (Becton Dickinson, Franklin Lakes, NJ). Data files were analyzed using FlowJo software (Tree Star, San Carlos, CA).

**Fig. 2** Mesodermal cell differentiation from iPSCs. **a** Flow cytometric analysis of mesodermal cells from all five iPSC lines at days 4, 5, and 6 during the course of EB culture. Lateral mesodermal cells were evaluated based on lack of expression of the surface marker E-cadherin (CD324, epithelial cadherin) and expression of Flk1 (CD309, VEGFR2) (*upper panel*). Paraxial mesodermal cells were evaluated based on lack of expression of E-cadherin and expression of PDGFRα (*lower panel*). **b** Quantitative real-time PCR analysis was used to detect the mesodermal markers *Flk1*, *Tbx6* and *Brachyury* at day 4 of EB culture. Data was normalized to *β-actin* expression

### Quantitative Real-Time PCR

Total RNA was isolated with the RNAqueous-Micro Kit (Ambion, Austin, TX). A high-capacity cDNA Archive kit (Applied Biosystems, Foster City, CA) was used to synthesize cDNA from mRNA. mRNA levels were normalized to *β-actin* as an internal control. In real-time PCR, mRNA levels were analyzed by the SYBR Green method with gene-specific primers or Taqman probe methods. Genes analyzed by SYBR Green included *Oct3/4* (Fw; gcagctcagccttaagaacatgt, Rv; cgatttgcatatctcctgaaggt), *Klf4* (Fw; gaactcacacaggcgagaaacc, Rv; tcggagcgggcgaatt), *Sox2* (Fw; atcaggctgccgagaatcc, Rv; ctcaaactgtgcataatggagt taaaaa) and *Nanog* (Fw; caaaaccaaaggatgaagtgcaa, Rv; gtgctgagcccttctgaatca). *Oct3/4*, *Klf4*, and *Sox2* primer sets recognized both internal and external sequences. Mouse *β-actin* (Fw; gctctggctcctagcaccat, Rv; gccaccgatccacacagagt) served as an internal control. Genes analyzed using the Taqman probe (Applied Biosystems) included *Flk1* (Mm01222421_m1), *Brachyury* (Mm01318252_m1), *Tbx6* (Mm00441681_m1), *Gata1* (Mm01352636_m1), *Klf1* (Mm00516096_m1), *CD45* (Mm01293577_m1), *Csf1r* (Mm01266652_m1), *PU.1* (Mm00488142_m1), and *c-Myc* (Mm00487804_m1). Mouse *β-actin* (4352933E) served as an internal control.

## Results

### Morphology and EB Formation Capacity of TTF-derived iPSCs

In this study, we cultured 5 induced pluripotent stem cell (iPSC) lines—256H13, 256H18, 212B2, 212D1, and 335D1—which were established by different protocols from adult mouse tail-tip fibroblasts (TTF) [6]. The *DsRed* gene is downstream of the *β-actin* (*ACTB*) gene in 256H13 and 256H18 iPSCs, whereas *GFP* is downstream of *Nanog* and serves an indicator of pluripotency in 212B2, 212D1, and 335D1 iPSCs, as summarized in Fig. 1a. *Oct3/4*, *Klf4*, *and Sox2* genes were transduced into TTFs to establish all iPSC lines, while the 212B2 line was also transduced with *c-Myc*. All iPSC colonies exhibited round morphology and exhibited large nucleoli and low cytoplasmic content.

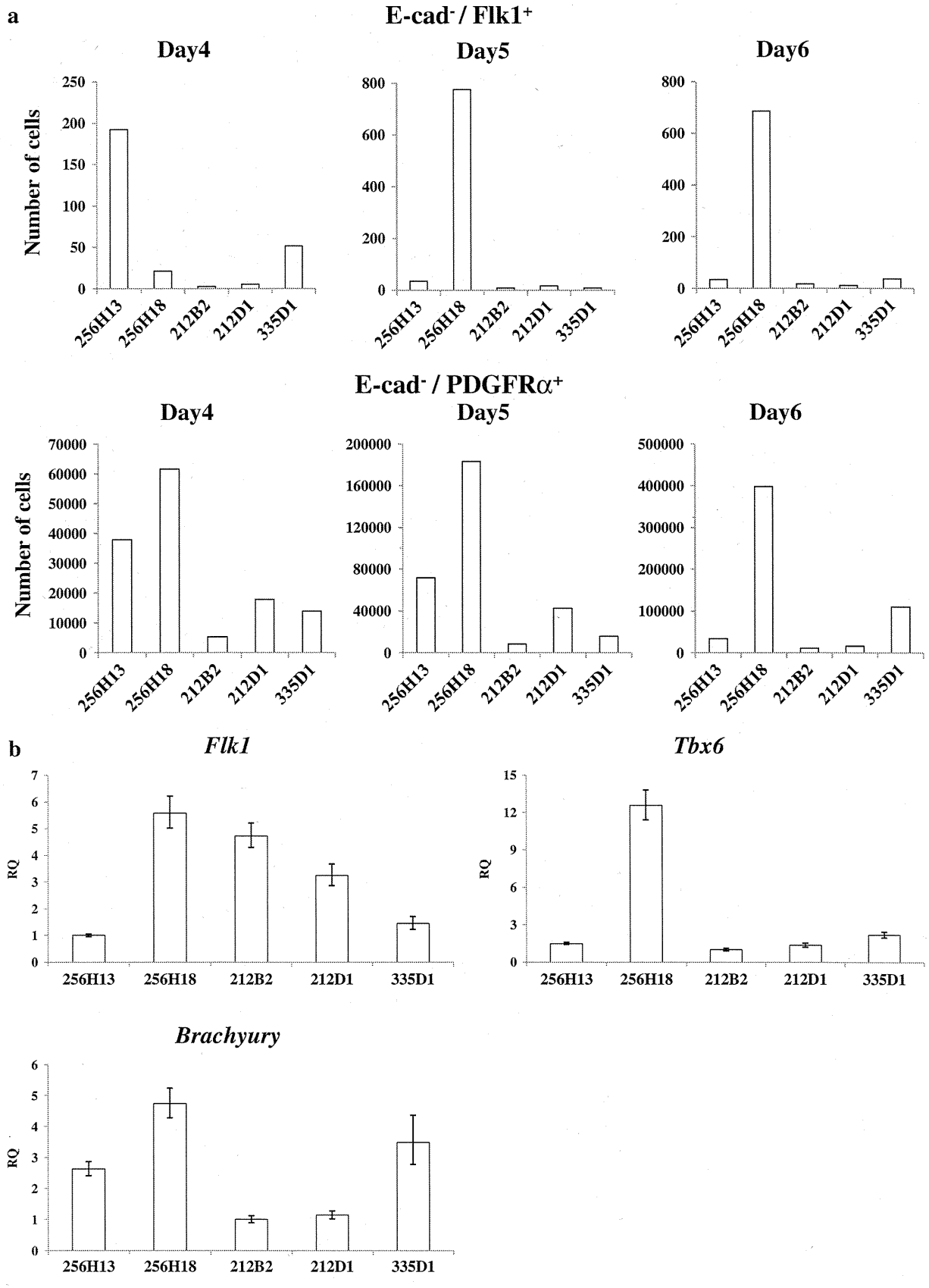
a
E-cad⁻ / Flk1⁺
Day4
Day5
Day6
Number of cells
250
200
150
100
50
0
800
600
400
200
0
256H13
256H18
212B2
212D1
335D1
E-cad⁻ / PDGFRα⁺
Day4
Day5
Day6
Number of cells
70000
60000
50000
40000
30000
20000
10000
0
200000
160000
120000
80000
40000
500000
400000
300000
200000
100000
b
Flk1
Tbx6
Brachyury
RQ
7
6
5
4
3
2
1
0
15
12
9
6
3
256H13
256H18
212B2
212D1
335D1

335D1 formed larger colonies than other lines (Fig. 1a). 212B2, 212D1and 335D1 lines were GFP-positive, indicative of *Nanog* expression and pluripotency.

Next, we performed differentiation culture using the method of embryoid body (EB) formation without cytokines (Supplementary Fig. 1a). Four, five and six days after EB formation, we observed the cultured cells microscopically (Fig. 1b) and evaluated proliferation by cell counting (Fig. 1c). All iPSCs formed EBs, although EB size and the number of adherent cells varied among lines (Fig. 1b). 212B2 and 335D1 iPSCs formed round EBs, although 335D1-derived EBs were larger than 212B2-derived EBs. By contrast, cultured 256H13, 256H18 and 212D1 iPSCs gave rise to adherent cells as well as round EBs. 256H18-derived EBs were larger than those derived from 212D1 cells at day 5 and, in the case of 256H18, adherent cells were observed most frequently (Fig. 1b). In terms of proliferation, the number of 256H13-derived cells increased at day 4 ($2.75\times10^5$ cells) and then plateaued. The number of 256H18 iPSCs also increased gradually through the culture period and then plateaued. 256H18 iPSCs-derived cells gradually increased during the culture and plateaued at day 5 ($4.70\times10^5$ cells). Although 212B2 and 335D1 lines increased gradually during the culture period, their viable cell number at day 6 ($1.69\times10^5$ and $3.63\times10^5$, respectively) was lower than that of 256H18 iPSCs. By contrast, the number of 212D2-derived cells increased from day 4 ($5.50\times10^4$ cells) to 5 ($1.70\times10^5$ cells), and then decreased ($1.19\times10^5$ cells). There was no significant difference among all iPSC lines in cell viability during EB culture (Supplementary Fig. 2). Taken together, our results indicate that EB formation and cell proliferation varies among five iPSC lines derived from the same tissue.

## Mesodermal Potential of TTF-derived iPSCs

To assess iPSC hematopoietic potential, we first examined their mesodermal potential, as hematopoietic cells are mesodermal in origin [13, 14]. ESC mesodermal differentiation was monitored using three markers: lack of E-cadherin (a marker of both ectoderm and endoderm in early mouse development [15]) expression, expression of platelet-derived growth factor receptor α (PDGFRα) and Flk1 (also known as VEGF receptor 2) [16, 17]. We compared the number of iPSC-derived E-cadherin$^-$/Flk1$^+$ cells, representing lateral mesoderm, and E-cadherin$^-$/PDGFRα$^+$ cells, representing paraxial mesoderm, at days 4, 5 and 6 of EB culture, since ESC-derived EBs [18, 19] contain Flk1$^+$ mesodermal cells at 4 to 4.5 days of culture and iPSC-derived EBs contain Flk1$^+$ cells at 5 days of culture [12]. The emergence of E-cadherin$^-$/Flk1$^+$ cells from the 256H13 line was the most rapid among the five lines tested, and the number of cells in this fraction was highest at day 4 (193 cells) and then decreased (Fig. 2a, upper panel). The number of E-cadherin$^-$/Flk1$^+$ cells from 256H18 was the highest among the five lines tested (day 5; 776 cells) (Fig. 2a, upper panel). In contrast, the number of 212B2 and 212D1 iPSC-derived E-cadherin$^-$/Flk1$^+$ cells was lower than that seen in the other three lines. The number of E-cadherin$^-$/PDGFRα$^+$ cells from 256H18 was highest among the five lines (day 6; $3.97\times10^5$ cells) (Fig. 2a, lower panel). The number of E-cadherin$^-$/PDGFRα$^+$ cells from 256H13 and 212D1 lines increased from days 4 to 5 and then decreased, whereas those from 256H18 and 212B2 lines gradually increased from days 4 to 6. The number of E-cadherin$^-$/PDGFRα$^+$ cells from 335D1 dramatically increased from day 5 ($1.59\times10^4$ cells) to day 6 ($1.10\times10^5$ cells) (Fig. 2a, lower panel). To confirm iPSC mesodermal cell differentiation, we employed PCR to examine expression of the mesoderm markers *Flk1* (lateral mesoderm), *Tbx6* [20] (paraxial mesoderm) and *Brachyury* [21] (pan-mesodermal marker). *Flk1* expression was lowest in 256H13-derived cells at day 4 of culture (Fig. 2b), whereas it was highest in 256H18-derived cells over days 4 to 6 (Supplementary Fig. 3 and 5). *Tbx6* expression at day 4 was highest in 256H18-derived iPSCs, whereas *Tbx6* expression was highest at days 5 and 6 in 335D1- and 256H13-derived cells, respectively (Fig. 2b and Supplementary Fig. 3 and 5). *Brachyury* expression at day 4 was higher in 256H18- and 335D1-derived cells compared to others (Fig. 2b), whereas it was highest at days 5 and 6 in 335D1- and 256H13-derived cells, similar to *Tbx6* expression (Supplementary Fig. 3 and 5). There was a trend in mesodermal differentiation. Early differentiation in 256H13 cells was observed, whereas late differentiation in 335D1 (Fig. 2a). 256H18 cells differentiated into both lateral and paraxial mesoderm most frequently. Overall differences we observed in mesodermal differentiation potential suggest variation in mesodermal potential of adult skin-derived induced pluripotent stem cell lines in mice.

**Fig. 3** Hematopoietic cell differentiation from iPSCs. **a** Differentiated iPSCs were collected at day 9 of EB culture and Ter119$^+$ erythroid cells were evaluated by flow cytometry. **b** Quantitative real-time PCR analysis was used to detect expression of the erythroid genes *Gata1* and *Klf1* at day 9 of EB culture. Data was normalized to *β-actin* expression. **c**, **d** Differentiated iPSCs were collected at day 9 of EB culture and evaluated by flow cytometry for (**c**) CD45$^+$ leukocytes and (**d**) myeloid cells (Mac1$^+$/F4/80$^+$ macrophages and Gr-1$^+$/F4/80$^-$ granulocytes). **e** Quantitative real-time PCR analysis was used to detect expression of the myeloid-related genes *CD45, Csf1r* and *PU.1* at day 9 of EB culture. Data was normalized to *β-actin* expression

## Hematopoietic Potential of TTF-derived iPSCs

Next we examined cell number and the percentage of erythroid and myeloid cells emerging during EB formation at day 9 of culture in the presence of cytokines (Supplementary Fig. 1b). Flow cytometry analysis showed that

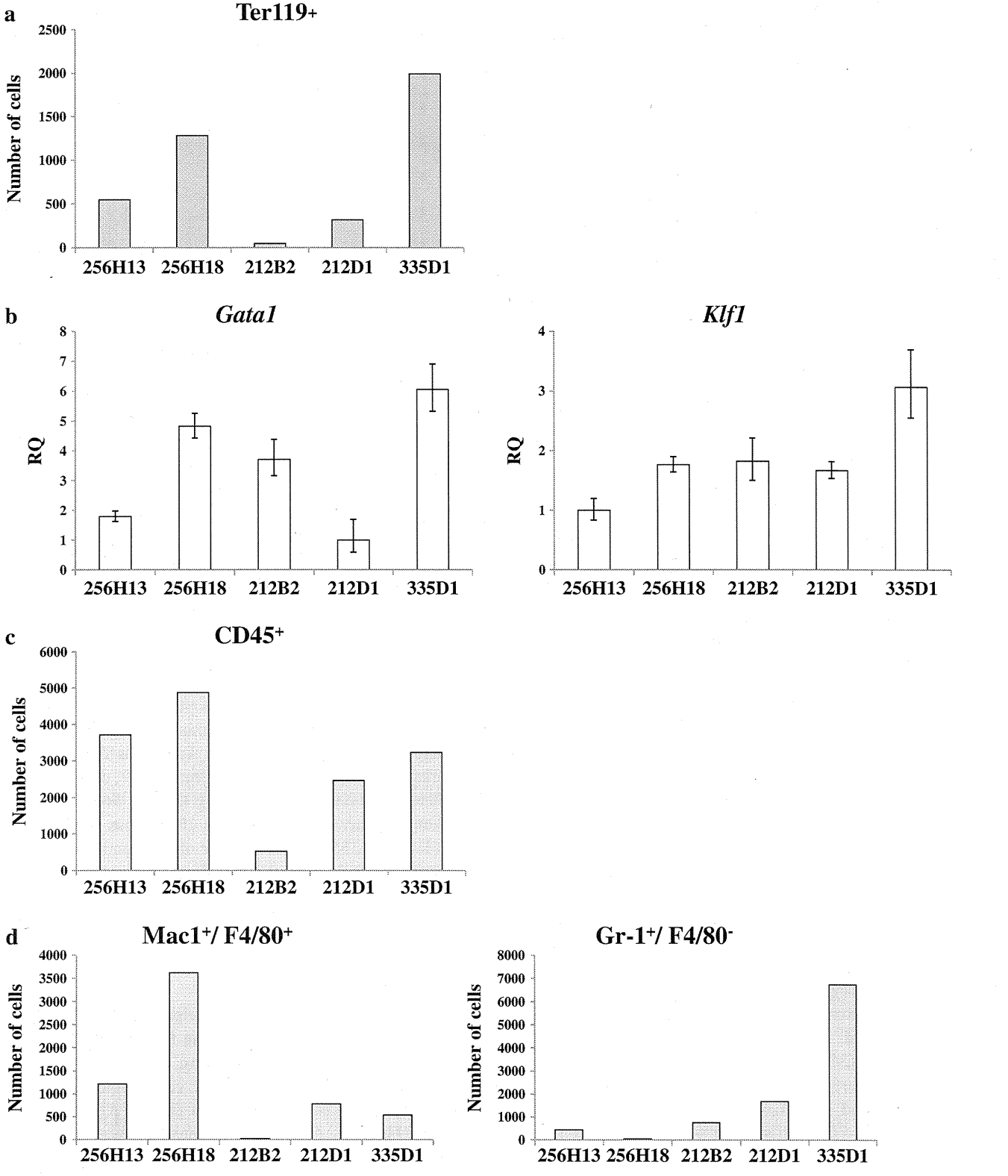
a
Ter119+
Number of cells
2500
2000
1500
1000
500
0
256H13 256H18 212B2 212D1 335D1
b
Gata1
RQ
8
7
6
5
4
3
2
1
0
256H13 256H18 212B2 212D1 335D1
Klf1
RQ
4
3
2
1
0
256H13 256H18 212B2 212D1 335D1
c
CD45+
Number of cells
6000
5000
4000
3000
2000
1000
0
256H13 256H18 212B2 212D1 335D1
d
Mac1+/ F4/80+
Number of cells
4000
3500
3000
2500
2000
1500
1000
500
0
256H13 256H18 212B2 212D1 335D1
Gr-1+/ F4/80-
Number of cells
8000
7000
6000
5000
4000
3000
2000
1000
0
256H13 256H18 212B2 212D1 335D1

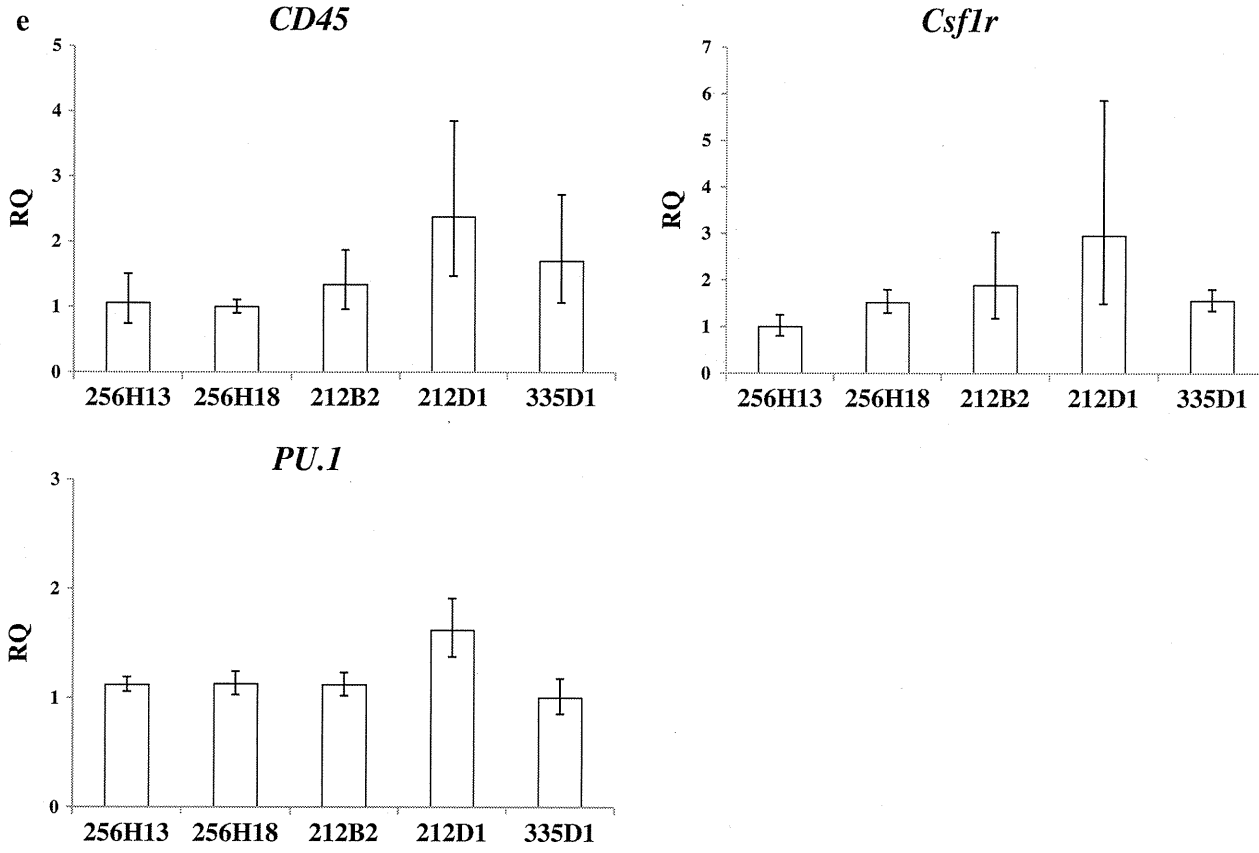


**Fig. 3** (continued)

lines 256H18 and 335D1 efficiently differentiated into Ter119$^+$ erythroid cells at 0.35% (1280 cells) and 0.72% (1991 cells), respectively. By contrast, 212B2 cells differentiated into Ter119$^+$ cells at low frequency (46 cells, 0.12%) (Fig. 3a, Supplementary Fig. 4a). In agreement, real-time PCR analysis showed that expression of the erythropoietic transcription factors *Gata1* [22] and *Klf1* [23] was the highest in 335D1 cells (6.05 times higher than in 212D1 cells and 3.07 times higher than in 256H13 cells) (Fig. 3b). 256H18 and 335D1 cells differentiated into CD45$^+$ leukocytes at 1.32% (4880 cells) and 1.17% (3229 cells), respectively (Fig. 3c, Supplementary Fig. 4b).

Flow cytometry analysis showed that 256H18 cells differentiated into Mac1$^+$/F4/80$^+$ macrophages at high frequency (3622 cells, 0.98%) (Fig. 3d, left panel; Supplementary Fig. 4c, left panel), whereas 335D1 cells differentiated into Gr-1$^+$/F4/80$^-$ granulocytes at high frequency (6738 cells, 2.45%) (Fig. 3d, right panel; Supplementary Fig. 4c, right panel). By contrast, 212B2 cells, which are transduced with the *c-Myc* gene, differentiated into CD45$^+$ leukocytes, Mac1$^+$/F4/80$^+$ macrophages and Gr-1$^+$/F4/80$^-$ granulocytes at low frequency (523, 20 and 756 cells, respectively) (Fig. 3c, d). When we analyzed expression of the leukocyte marker *CD45*, *Csf1r* (encoding colony stimulating factor 1 receptor, a macrophage marker), and *PU.1* (also known as *Spi-1*, which marks the myeloid lineage) at culture day 9, no significant differences were observed among the five lines (Fig. 3e). Taken together, among the five iPSC lines tested, only 256H18 and 335D1 were capable of differentiating at high frequency into both erythroid cells and leukocytes at day 9 of culture.

## Expression of Reprogramming and Pluripotency Genes During EB Formation from iPSCs

We next investigated whether pluripotency of iPSCs was related to the nature reprogramming factors used transduce somatic cells. Prior to initiating EB culture, *c-Myc* expression was highest in 212B2 cells, which had been transduced with *c-Myc* along with *Oct3/4*, *Klf4* and *Sox2* genes (Fig. 4a). *Oct3/4* gene expression was highest in 256H13 cells, whereas *Klf4*, *Sox2* and *Nanog* gene expression did not significantly differ among the lines prior to culture. *Oct3/4*, *Klf4* and *Sox2* expression at day 4 of culture was the highest in 212B2 cells, suggesting that they retain pluripotency longer than do the other lines (Fig. 4b).

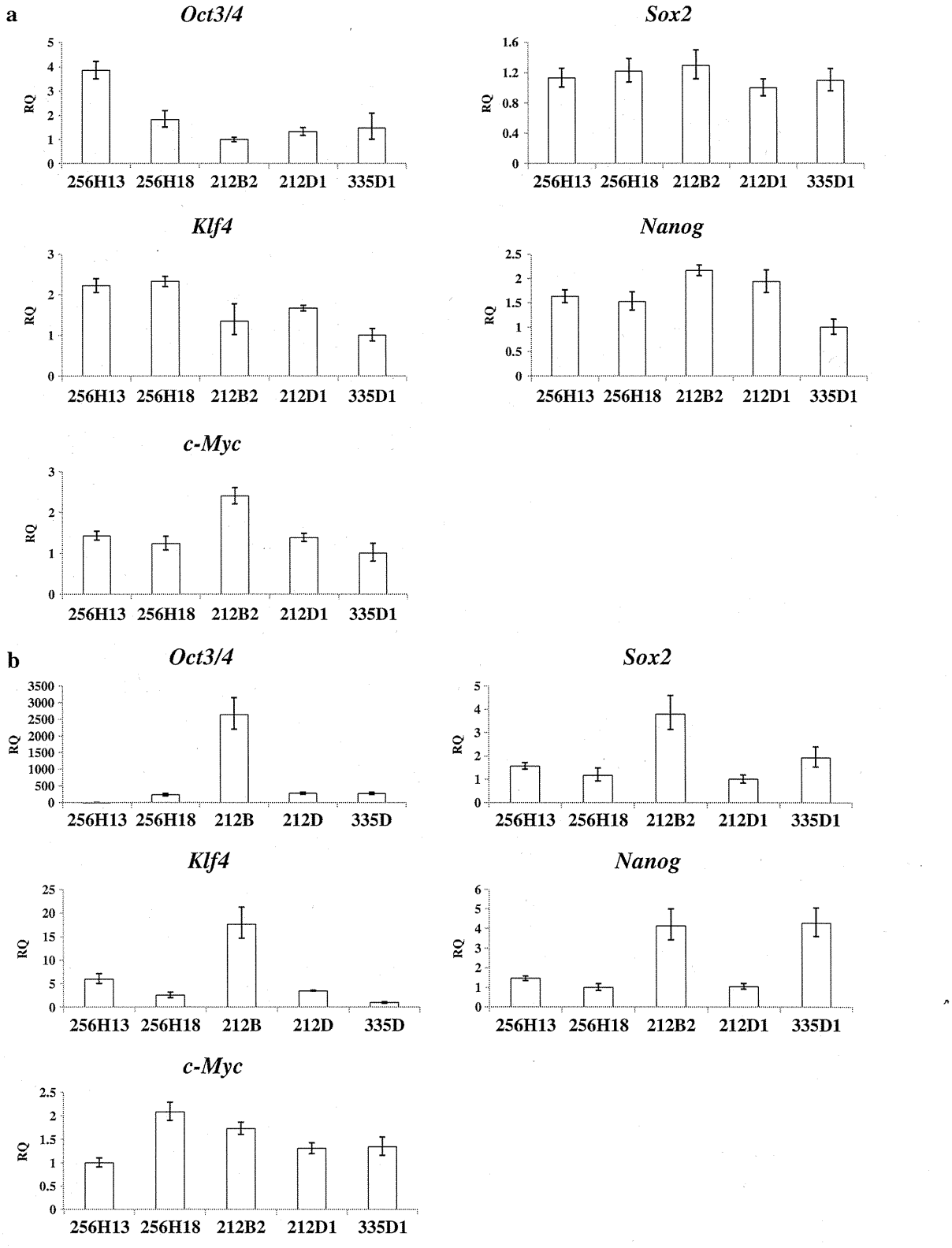


**Fig. 4** Comparison of reprogramming and pluripotency gene expression. Quantitative real-time PCR analysis was used to detect expression of the reprogramming genes *Oct3/4, Klf4, Sox2* and *c-Myc* and the pluripotency gene *Nanog* at days 0 (**a**) and 4 (**b**) of EB culture. Data was normalized to *β-actin* expression

## Discussion

iPSCs constitute important tools for future regenerative medicine. In this study we compared mesodermal and hematopoietic potential of several iPSC lines, since differentiation potential reportedly varies among iPSC lines established by different sources and methods [12]. Although all iPSCs possessed pluripotency, as defined by expression of *Oct3/4* and *Nanog*, each line showed variations in EB formation and cell proliferation. Examination of mesodermal potential using both flow cytometry and real-time PCR methods, confirmed these differences: specifically, the 256H18 iPSC line gave rise to mesodermal cells at high frequency, whereas 212B2 cells showed the lowest frequency. To identify factors underlying mesodermal potential, we compared expression of both differentiation and pluripotency markers. As summarized in Supplementary Fig. 5, expression of the differentiation markers *Flk1*, *Tbx6*, and *Brachyury* in 256H18 iPSCs was highest at day 4 of culture. Although there was no significant correlation between mesodermal potential and expression of pluripotency markers (Fig. 4), the number of EBs is likely positively correlated with mesodermal potential (Fig. 1). In terms of hematopoietic potential, variations in differentiation capacity were confirmed by flow cytometric and real-time PCR analyses. 256H18 and 335D1 iPSCs generated erythroid cells and leukocytes at high frequency, whereas a low frequency was seen with 212B2 cells (Fig. 3). Expression of the *Oct3/4*, *Sox2*, *Klf4* and *Nanog* pluripotency genes in 256H18 was lowest, whereas 212B2 iPSCs showed highest expression of *Oct3/4*, *Sox2* and *Klf4*. Given the results of our hematopoietic cell differentiation assays at day 4 of culture, these results suggest an inverse relationship between hematopoietic potential and pluripotency gene expression (Fig. 4). *c-Myc* expression in 212B2 cells was highest before culture (Fig. 4a), likely due to ectopic transduction of *c-Myc*. There was a correlation between high *c-Myc* expression and low induction of mesodermal and hematopoietic cells. In our culture conditions, *c-Myc* likely down-regulates mesodermal and hematopoietic cell induction from the 212B2 iPSC line. Our results are compatible with previous reports mentioning that *c-Myc* maintains pluripotency of ESCs [24] and iPSCs [25], and similar to the report showing that c-Myc down-regulates cardiogenic [26] and endodermal differentiation [25] of iPSCs. Taken together, our results imply that iPSCs lacking *c-Myc* transduction will be preferably used for clinical purposes.

Passage number of iPSCs reportedly affected the hematopoietic differentiation [27]. As passage number of iPSCs increased, the transient epigenetic memory of their original somatic cells was gradually lost and hematopoietic differentiation capacity was up-regulated in TTF-derived iPSCs [27]. 256H18 and 335D1 iPSCs generated hematopoietic cells at high frequency, whereas a low frequency was seen in 212B2 in our culture condition (Fig. 3). Since we used iPSC lines of 256H18, 335D1 and 212B2 with similar passage number (P.8- P.10), it is unlikely that passage number affected the hematopoietic differentiation capacity among these three lines. Concerning the other 2 iPSC lines, passage number was lower in 256H13 (P.6-P.9) and 212D1 (P.6) than in 256H18, 335D1 and 212B2. Less hematopoietic cell differentiation in 256H13 and 212D1 than 256H18 and 335D1 was might be due to the difference of passage number.

Taken together, even derived from the same TTF origin, each iPSC demonstrated different mesodermal and hematopoietic potential. Transduction method with retroviral infection and transfection efficiency (20–30%) were similar, while *c-Myc* gene transduction, drug selection with puromycin, reporter genes (Actb-DsRed or Nanog-GFP) and passage number were not identical among five iPSC lines. Therefore, variation in mesodermal and hematopoietic potential was likely affected by combination of transduced genes and passage number, but not transfection methods, drug selection and reporter genes.

Recently, it was reported that iPSCs can be established from peripheral blood (PB) cells [28]. Since collecting a PB sample from a patient is practically easier than taking skin fibroblasts by biopsy in terms of risk and pain, it will be further necessary to evaluate the hematopoietic potential of PB-derived iPSCs in both mice and humans.

**Acknowledgements** This work was supported by a grant from the Project for Realization of Regenerative Medicine from the Ministry of Education, Culture, Sports, Science and Technology and by a grant from the BASIS project from the Ministry of Education, Culture, Sports, Science and Technology. T. Inoue and K. Kulkeaw is supported by research fellowships from the Ministry of Education, Culture, Sports, Science and Technology, and from The Tokyo Biochemical Research Foundation, respectively. We thank Dr. Keisuke Okita, Ms. Yuka Horio, Ms. Chiyo Mizuochi and the Research Support Center, Graduate School of Medical Sciences, Kyushu University for technical supports, and Dr. Minetaro Ogawa and Dr. Hiroshi Sakamoto for providing LIF. All iPSCs were kindly provided by Dr. Shinya Yamanaka.

**Author Contributions** Tomoko Inoue performed the experiments, analyzed data and wrote the manuscript. Kasem Kulkeaw, Satoko Okayama and Kenzaburo Tani performed the experiments. Daisuke Sugiyama designed the experiments and wrote the manuscript.

**Conflict of Interest** All disclosures will be published when the manuscript is accepted.

## References

1. Takahashi, K., & Yamanaka, S. (2006). Induction of pluripotent stem cells from mouse embryonic and adult fibroblast cultures by defined factors. *Cell, 126*, 663–676.
2. Wernig, M., Meissner, A., Foreman, R., et al. (2007). In vitro reprogramming of fibroblasts into a pluripotent ES-cell-like state. *Nature, 448*, 318–324.

3. Okita, K., Ichisaka, T., & Yamanaka, S. (2007). Generation of germline-competent induced pluripotent stem cells. *Nature, 448*, 313–317.
4. Yu, J., Vodyanik, M. A., Smuga-Otto, K., et al. (2007). Induced pluripotent stem cell lines derived from human somatic cells. *Science, 318*, 1917–1920.
5. Nelson, T. J., Martinez-Fernandez, A., Yamada, S., Mael, A. A., Terzic, A., & Ikeda, Y. (2009). Induced pluripotent reprogramming from promiscuous human stemness related factors. *Clinical and Translational Science, 2*, 118–126.
6. Nakagawa, M., Koyanagi, M., Tanabe, K., et al. (2008). Generation of induced pluripotent stem cells without Myc from mouse and human fibroblasts. *Nature Biotechnology, 26*, 101–106.
7. Stadtfeld, M., Brennand, K., & Hochedlinger, K. (2008). Reprogramming of pancreatic beta cells into induced pluripotent stem cells. *Current Biology, 18*, 890–894.
8. Okita, K., Nakagawa, M., Hyenjong, H., Ichisaka, T., & Yamanaka, S. (2008). Generation of mouse induced pluripotent stem cells without viral vectors. *Science, 322*, 949–953.
9. Aoi, T., Yae, K., Nakagawa, M., et al. (2008). Generation of pluripotent stem cells from adult mouse liver and stomach cells. *Science, 321*, 699–702.
10. Hanna, J., Markoulaki, S., Schorderet, P., et al. (2008). Direct reprogramming of terminally differentiated mature B lymphocytes to pluripotency. *Cell, 133*, 250–264.
11. Takenaka, C., Nishishita, N., Takada, N., Jakt, L. M., & Kawamata, S. (2010). Effective generation of iPS cells from CD34+ cord blood cells by inhibition of p53. *Experimental Hematology, 38*, 154–162.
12. Kulkeaw, K., Horio, Y., Mizuochi, C., Ogawa, M., & Sugiyama, D. (2010). Variation in hematopoietic potential of induced pluripotent stem cell lines. *Stem Cell Reviews, 6*, 381–389.
13. Huber, T. L., Kouskoff, V., Fehling, H. J., Palis, J., & Keller, G. (2004). Haemangioblast commitment is initiated in the primitive streak of the mouse embryo. *Nature, 432*, 625–630.
14. Lengerke, C., Grauer, M., Niebuhr, N. I., et al. (2009). Hematopoietic development from human induced pluripotent stem cells. *Annals of the New York Academy of Sciences, 1176*, 219–227.
15. Era, T., Izumi, N., Hayashi, M., Tada, S., & Nishikawa, S. (2008). Multiple mesoderm subsets give rise to endothelial cells, whereas hematopoietic cells are differentiated only from a restricted subset in embryonic stem cell differentiation culture. *Stem Cells, 26*, 401–411.
16. Kataoka, H., Takakura, N., Nishikawa, S., et al. (1997). Expressions of PDGF receptor alpha, c-Kit and Flk1 genes clustering in mouse chromosome 5 define distinct subsets of nascent mesodermal cells. *Development, Growth & Differentiation, 39*, 729–740.
17. Sakurai, H., Era, T., Jakt, L. M., Okada, M., Nakai, S., & Nishikawa, S. (2006). In vitro modeling of paraxial and lateral mesoderm differentiation reveals early reversibility. *Stem Cells, 24*, 575–586.
18. Choi, K., Kennedy, M., Kazarov, A., Papadimitriou, J. C., & Keller, G. (1998). A common precursor for hematopoietic and endothelial cells. *Development, 125*, 725–732.
19. Fehling, H. J., Lacaud, G., Kubo, A., et al. (2003). Tracking mesoderm induction and its specification to the hemangioblast during embryonic stem cell differentiation. *Development, 130*, 4217–4227.
20. Chapman, D. L., Agulnik, I., Hancock, S., Silver, L. M., & Papaioannou, V. E. (1996). Tbx6, a mouse T-Box gene implicated in paraxial mesoderm formation at gastrulation. *Developmental Biology, 180*, 534–542.
21. Wilkinson, D. G., Bhatt, S., & Herrmann, B. G. (1990). Expression pattern of the mouse T gene and its role in mesoderm formation. *Nature, 343*, 657–659.
22. Whitelaw, E., Tsai, S. F., Hogben, P., & Orkin, S. H. (1990). Regulated expression of globin chains and the erythroid transcription factor GATA-1 during erythropoiesis in the developing mouse. *Molecular and Cellular Biology, 10*, 6596–6606.
23. Miller, I. J., & Bieker, J. J. (1993). A novel, erythroid cell-specific murine transcription factor that binds to the CACCC element and is related to the Kruppel family of nuclear proteins. *Molecular and Cellular Biology, 13*, 2776–2786.
24. Varlakhanova, N. V., Cotterman, R. F., & deVries, W. N. (2010). Myc maintains embryonic stem cell pluripotency and self-renewal. *Differentiation, 80*, 9–19.
25. Smith, K. N., Singh, A. M., & Dalton, S. (2010). Myc represses primitive endoderm differentiation in pluripotent stem cells. *Cell Stem Cell, 7*, 343–54.
26. Martinez-Fernandez, A., Nelson, T. J., Ikeda, Y., & Terzic, A. (2010). c-MYC independent nuclear reprogramming favors cardiogenic potential of induced pluripotent stem cells. *Journal of Cardiovascular Translational Research, 3*, 13–23.
27. Polo, J. M., Liu, S., & Figueroa, M. E. (2010). Cell type of origin influences the molecular and functional properties of mouse induced pluripotent stem cells. *Nature Biotechnology, 28*, 848–55.
28. Loh, Y. H., Agarwal, S., & Park, I. H. (2009). Generation of induced pluripotent stem cells from human blood. *Blood, 113*, 5476–9.